metals

MDPI

Review

Reoxidation Behavior of the Direct Reduced Iron and Hot Briquetted Iron during Handling and Their Integration into Electric Arc Furnace Steelmaking: A Review

Lina Kieush [1,*], Stefanie Lesiak [1], Johannes Rieger [1], Melanie Leitner [1], Lukas Schmidt [1] and Oday Daghagheleh [2]

[1] K1-MET GmbH, Stahlstrasse 14, 4020 Linz, Austria
[2] Chair of Ferrous Metallurgy, Montanuniversität Leoben, Franz-Josef-Str. 18, 8700 Leoben, Austria
* Correspondence: lina.kieush@k1-met.com

Abstract: This paper studies the integration of direct reduced iron (DRI) and hot briquetted iron (HBI) into the steelmaking process via an electric arc furnace (EAF). Considering a variety of DRI production techniques distinguished by different reactor types, this paper provides a comparative overview of the current state. It delves into significant challenges, such as the susceptibility of DRI to reoxidation and the necessity of thorough handling to maintain its quality. The effectiveness of several reoxidation mitigation strategies, including the application of thin oxide layers, briquetting, various coatings, and nitride formation in ammonia-based reduction processes, is evaluated. Most existing studies have primarily focused on the reoxidation of DRI rather than on HBI, despite the fact that HBI may undergo reoxidation. The importance of DRI/HBI in offering an alternative to the integrated steelmaking route is highlighted, focusing on how it changes the EAF process compared to those for melting scrap. This paper also identifies several research prospects for further DRI/HBI applications in steel production.

Keywords: direct reduced iron; hot briquetted iron; reoxidation; electric arc furnace; steelmaking

Citation: Kieush, L.; Lesiak, S.; Rieger, J.; Leitner, M.; Schmidt, L.; Daghagheleh, O. Reoxidation Behavior of the Direct Reduced Iron and Hot Briquetted Iron during Handling and Their Integration into Electric Arc Furnace Steelmaking: A Review. *Metals* **2024**, *14*, 873. https://doi.org/10.3390/met14080873

Academic Editor: Noé Cheung

Received: 2 July 2024
Revised: 25 July 2024
Accepted: 28 July 2024
Published: 29 July 2024

1. Introduction

The direct reduction (DR) of iron ore (in the form of lumps, pellets, or fines) is a process of forming low-valence oxides in the production of direct reduced iron (DRI), also known as sponge iron [1,2], where oxygen is removed from iron ore below the melting point of reactants and products, applying different reductants, namely from the conversion of natural gas (NG), syngas [3], byproduct gases [4,5], coal [6], hydrogen (H_2) [7], etc. The emissions intensity of DR varies with the chosen reductant, driven by factors such as gas accessibility, costs, and the requirement for high-grade iron ore. High-grade ore is important for DRI technology, yet it makes up less than 5% of the global iron ore supply [8]. Coal-based DRI reduces carbon dioxide (CO_2) emissions by 38%, contrasted with blast furnace-basic oxygen furnace (BF-BOF) ironmaking. Using a combination gas of methane (CH_4), H_2, and carbon monoxide (CO) for DRI reduces CO_2 emissions by 61% as opposed to BF-BOF [9]. In comparison with the NG-based DR process, using H_2 can reduce up to 91% of directly emitted CO_2, not accounting for the CO_2 intensity of the additional electricity required [10]. However, this value also hinges on the method used for H_2 production and its associated CO_2 footprint.

Different reactor technologies are used for DRI production, such as shaft furnaces, rotary kiln (RK), rotary hearth furnaces (RHF), and fluidized bed reactors. However, 96.8% of the DRI is produced using two technologies, while 72.4% is attributed to shaft furnaces and 24.4% to rotary kilns (RK) [11]. In 2022, the worldwide production of DRI reached 127.36 million tons (Mt), marking an increase of nearly 6.9% over the prior record of 119.2 Mt established in 2021. Within the spectrum of DRI approaches, MIDREX® led with

approximately 57.8% of the global DRI output for the year. In comparison, other gas-based technologies contributed 12.1% from HYL/ENERGIRON® and 2.2% from PERED. The remaining production primarily involved coal-based DR processes in RK, accounting for 27.9% [12].

DRI is an alternative for the iron production industry [13,14]. In addition, DRI can be compacted to reduce porosity and converted to hot briquetted iron (HBI) [15]. This process not only prevents reoxidation but also enables HBI to be transported over long distances and stored outside for long periods. However, cases of reoxidation of HBI might also occur.

The electric arc furnace (EAF) is well-suited to integrating DRI/HBI owing to its flexibility in charge materials. EAF can melt steel scrap, DRI/HBI, or a combination of both. With the utilization of scrap in the BF-BOF and EAF steelmaking processes, the available supply of scrap metal is becoming more limited [15,16].

In the EAF, since DRI has a higher bulk density than most steel scrap types, surpassing slag density, this characteristic promotes its melting at the interface between slag and metal. The remaining wuestite (FeO) content in DRI interacts with the carbon in the liquid metal, enhancing the formation of foaming slag that protects the refractory lining from the electric arcs. Nonetheless, controlling the rate at which DRI is introduced into the EAF is important. The feeding rate varies, influenced by the chemical composition and metallization degree of DRI, the temperature of the metal bath, an initial amount of liquid steel (LS) bath, and the mixing energy from the oxygen-carbon injectors along with the stirring [17]. This rate typically falls within a range of 27–35 $kg \cdot (min \cdot MW)^{-1}$ [16]. Most DRI/HBI can be melted with a varying share of steel scrap in EAF. The specific CO_2 emissions are within the range of 0.9–1.8 $t_{CO2} \cdot t_{LS}{}^{-1}$, including local CO_2 intensity of electrical energy for EAF [18,19].

Furthermore, there are other perspectives, including flexibility, quality control, and resource optimization, that should be considered, including the important environmental aspect. Adding DRI to the EAF allows for more precise control over the final composition of steel. This is necessary for producing high-quality steel grades that meet strict specifications for alloy content and impurity levels. Additionally, using DR might enable the efficient use of iron ore resources, including low-grade iron ores unsuitable for some metallurgical processes. Although applying the proportion of DRI or HBI for EAF is attractive, it may pose issues that should be addressed.

The focus of this paper lies in considering and showing the primary outcomes and aspects associated with DRI or HBI, starting with the characteristics and comparison of available main types of reduction reactors. This study evaluates the current research state, focusing on challenges such as reoxidation of DRI or HBI that may arise post-production and exploring potential solutions for handling and transportation. To the best of our knowledge, existing review papers related to the topic of DRI and HBI have not focused on the challenges related to reoxidation, revealing the necessity for further research. Moreover, the paper discusses the research results on applying DRI or HBI into EAF under laboratory and industrial scale from the process-wise perspective, assesses their impact and limitations, and suggests areas for future research.

The review is organized as follows: Section 2 presents the main principles, routes, and reactors comparison of the DR process, along with the resulting DRI characteristics; Section 3 discusses the carburization phenomenon that might occur during or after the reduction process; Section 4 focuses on the reoxidation issue and summarises the current state of the existing methods for mitigating this effect; Section 5 contains generalized measurements concerning storage, handling, and transportation; Section 6 comprises current research results concerning DRI or HBI application in an EAF steelmaking, considering the effect on this process; and Section 7 presents summary and research prospects.

2. Direct Reduction of Iron Ore

2.1. Main Principles of DR

The principles of the DR of iron ore have been outlined [20–22], and several points can be mentioned. The initial stage of reduction typically involves hematite (Fe_2O_3), which is

first converted into magnetite (Fe_3O_4), followed by a reduction to FeO. Iron oxide reduction shows a broad range of possible reactions before its final reduction to metallic iron, according to Equations (1)–(8). FeO frequently shows non-stoichiometry, characterized by a cation deficiency represented as $Fe_{(1-x)}O$. Nevertheless, to simplify the reaction equations (specifically Equations (2), (3), (6) and (7)), FeO is depicted without considering the precise stoichiometric ratio. The process of DR in a CO atmosphere often results in carbon deposition, a consequence of the inverse Boudouard reaction (CO disproportionation reaction) at temperatures below 1000 °C, along with the Beggs reaction [23,24], according to Equations (9) and (10). The Beggs reaction and the CO disproportionation reaction, both exothermic, generate H_2O or CO_2. This leads to a decrease in the quality of the gas within the reactor, thereby making the conditions less favorable for reduction processes [25].

$$3Fe_2O_3\,(s) + CO\,(g) \leftrightarrow 2Fe_3O_4\,(s) + CO_2\,(g),\ \Delta H^{\theta}_{298K} = -43\ kJ{\cdot}mol^{-1}, \quad (1)$$

$$Fe_3O_4\,(s) + CO\,(g) \leftrightarrow 3FeO\,(s) + CO_2\,(g),\ \Delta H^{\theta}_{298K} = 19\ kJ{\cdot}mol^{-1}, \quad (2)$$

$$FeO\,(s) + CO\,(g) \leftrightarrow Fe\,(s) + CO_2\,(g),\ \Delta H^{\theta}_{298K} = -11\ kJ{\cdot}mol^{-1}, \quad (3)$$

$$Fe_2O_3\,(s) + 3CO\,(g) \leftrightarrow 2Fe\,(s) + 3CO_2\,(g),\ \Delta H^{\theta}_{298K} = -23\ kJ{\cdot}mol^{-1}, \quad (4)$$

$$3Fe_2O_3\,(s) + H_2\,(g) \leftrightarrow 2Fe_3O_4\,(s) + H_2O\,(g),\ \Delta H^{\theta}_{298K} = -2\ kJ{\cdot}mol^{-1}, \quad (5)$$

$$Fe_3O_4\,(s) + H_2\,(g) \leftrightarrow 3FeO\,(s) + H_2O\,(g),\ \Delta H^{\theta}_{298K} = 60\ kJ{\cdot}mol^{-1}, \quad (6)$$

$$FeO\,(s) + H_2\,(g) \leftrightarrow Fe\,(s) + H_2O\,(g),\ \Delta H^{\theta}_{298K} = 30\ kJ{\cdot}mol^{-1}, \quad (7)$$

$$Fe_2O_3\,(s) + 3H_2\,(g) \leftrightarrow 2Fe\,(s) + 3H_2O\,(g),\ \Delta H^{\theta}_{298K} = 100\ kJ{\cdot}mol^{-1}, \quad (8)$$

$$2CO\,(g) \leftrightarrow C\,(s) + CO_2\,(g),\ \Delta H^{\theta}_{298K} = -172\ kJ{\cdot}mol^{-1}, \quad (9)$$

$$CO\,(g) + H_2\,(g) \leftrightarrow C\,(s) + H_2O\,(g),\ \Delta H^{\theta}_{298K} = -131\ kJ{\cdot}mol^{-1}, \quad (10)$$

The metallization degree and the behavior of iron ore change based on the reducing atmosphere, temperature, and reduction rate [24]. The reduction process of Fe_2O_3 becomes unstable at temperatures under 570 °C [26]. At temperatures above 570 °C, the initial reduction phase (from Fe_2O_3 to Fe_3O_4) necessitates a mildly reducing atmosphere and is typically seen as an irreversible process [27]. Subsequent transformation from Fe_3O_4 to FeO is facilitated by both CO and H_2, and this step is endothermic. Below 570 °C, FeO does not form, leading to the DR of Fe_3O_4 to metallic iron.

Generally, the overall reduction of Fe_2O_3 by CO is exothermic, in contrast to the endothermic nature of H_2 reduction [28,29]. Typically, the highly endothermic nature of reduction systems necessitates the addition of extra energy to maintain a steady reduction temperature when using H_2.

The transition from FeO to Fe, the most challenging reaction, demands a highly reducing environment. Beyond 810 °C, the reducing capability of hydrogen surpasses that of CO [30], influenced by kinetic factors and the water-gas shift reaction. In addition, the reaction rate would increase with the higher H_2 content at temperatures above 1000 °C [31]. The reduction rates with H_2 are much faster, up to 10 times than those with CO [23,32,33]. Additionally, H_2 has a higher diffusion rate and could penetrate much deeper into the crystal structure of the iron oxide, leading to a higher reduction rate and a greater metallization degree [24].

From the kinetic perspective, reduction in shaft furnaces involves several sequential steps, with the overall rate being determined by the slowest of these steps. In a shaft furnace, reduction contains the flow of gas and solid phases, the exchange of mass and heat between these phases, and the reactions occurring at the interface between gas and solid. In general, these steps encompass the movement of gases to the reaction site, the chemical reaction itself, and removing reaction products from the site. Additionally, solid-state diffusion can play a role, such as when FeO is being reduced to iron and a gradient of ferrous iron is created, necessitating the movement of ferrous ions to the reaction site for further

conversion. Notably, temperature, pressure, flow rate, reducing gas composition, as well as size, morphology, free surface area, porosity, tortuosity, and chemical composition [23,34] of the materials involved are factors influencing the kinetics of the mentioned reactions. The reduction temperature varies, falling within the 850–960 °C range [26,35], and operating pressures utilizing NG range from 0.23 to 0.60 MPa [26].

Iron oxides are reduced across multiple stages in fluidized bed reactors, representing the counter-current flow of gas and solids seen in shaft furnaces. Initially, both the solids and reductant gas are heated in a preheater, ensuring they reach the first reduction chamber at temperatures conducive to offsetting the endothermic nature of the reduction process. The reduction usually occurs at temperatures ranging from 760 °C [36], when the DRI product may become pyrophoric, to 800 °C, where issues like sticking and de-fluidization might arise [37]. Operating pressures utilizing NG range from 1.1 to 1.3 MPa [26].

In RHF and RK, despite the occurrence of similar reactions, the mechanisms and rate-limiting steps differ. Reduction predominantly occurs within individual pellets that possess sufficient carbon to facilitate the reduction of iron oxide. RHF functions at higher temperatures of around 1300 °C [38] and typically features shorter residence times than RK, which operates at about 960–1100 °C [39] and atmospheric pressure. According to the study [38], achieving the highest reduction efficiency at 1250 °C for RHF requires an optimal carbon/Fe_2O_3 molar ratio of 1.66. Additionally, pellets reduced under these conditions demonstrated enhanced compressive strength.

2.2. Main Routes and Reactors for the DR Processes

The selection of raw materials optimal for DR in steelmaking is based on several principles: their chemical and physical properties, their ability to undergo reduction, and the overall cost-effectiveness encompassing both the DR process and subsequent steelmaking [40]. The DR process utilizes NG, which typically operates with vertical shaft furnaces and fluidized bed reactors (Figure 1). Meanwhile, coal, either directly or after the conversion process into syngas, can be utilized in DR processes in various systems, including vertical shaft furnaces [41], fluidized bed reactors [42,43], RHF [44], and RK [45,46].

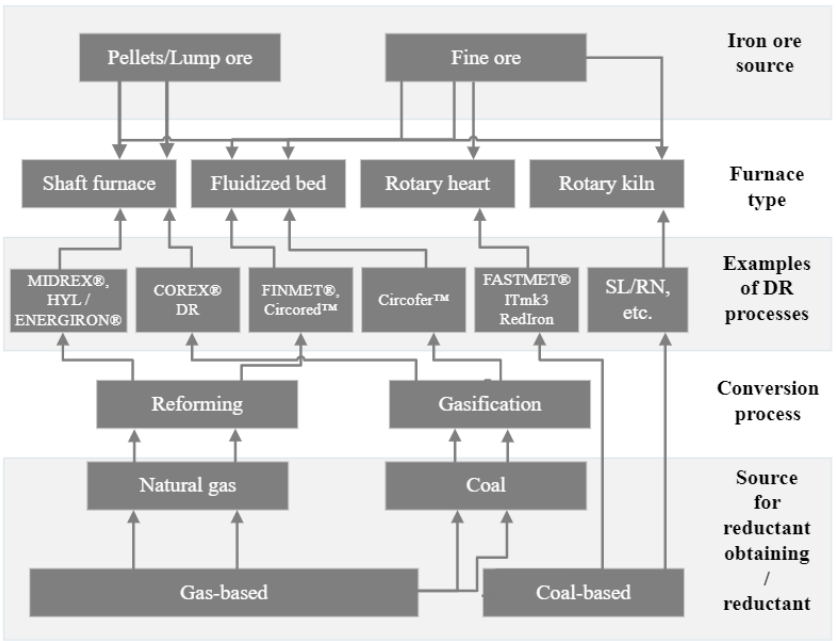

Figure 1. General overview of the main routes of direct reduction based on reductant and furnace type, adapted from Ref. [47].

The majority of DRI is produced in a shaft furnace [48,49], which necessitates a uniformly coarse feed. A shaft furnace is employed for processing pellets or lump ore. Given the high velocity of gases and the abrasive environment within shaft furnaces, fine particles are considered unsuitable for feedstock; such particles are likely to be removed by the gas stream, requiring subsequent collection and recirculation. Fluidized bed DR processes are exceptions, where iron ore, refined via ore-beneficiation, results in iron ore concentrate powder, which can be directly used [50]. Assuming a substantial number of studies have focused on examining and analyzing reactor types for DR, Table 1 provides a comparative overview of the primary DR reactors, as well as their main advantages and disadvantages.

Table 1. Comparison of main DR reactors, according to [9,15,51–57].

Furnace Type	Form of Reactant (Iron Ore)	Reductant	Short Description of the Process	Advantages	Disadvantages	Metallization Degree of the Product
Shaft furnace	Lump, pellets	Converted NG, syngas, H_2	A vertical furnace in which iron ore pellets or lumps are charged at the top, and reducing gas flows upward, reducing the iron oxides to iron. It relies on solid-gas reactions at high temperatures.	Large production capacity. High product quality.	Ore in pellet form should have a minimum of 67% Fe content. High cost of reducing gas.	≥92%
Fluidized bed	Fines	Converted NG, syngas, H_2	Iron ore particles are suspended in an upward-flowing stream of reducing gas, promoting high mass and heat transfer. Using a fluidizing medium enhances the reaction kinetics by increasing the contact surface area between the reducing gas and the iron ore particles.	Iron ore fines can be used without pelletizing and agglomeration. Fast reaction rate.	Complex structure of reactors. Particle sticking tendency.	≥92%
Rotary kiln	Lump, pellets	Coal (5–20 mm) and recycled char Char, coal	A kiln is a rotating cylindrical vessel through which lumps or pellets, along with coal or gas as a reductant, are passing. The kiln is slightly inclined to assist material flow. Reduction occurs in solid and gaseous phases; the rotating action promotes mixing and contact between ore and reducing agents, enhancing the reduction process.	Various types of coal can be used. Processing low-grade ores. Flexible structure of the reactor.	Significant levels of impurities, including sulfur. Slow reaction rate. Significant energy usage. Problems with kiln lining agglomeration.	≥90%
Rotary hearth furnace	Composite pellets (16–22 mm) Composite pellets	Coal (70% below 45 µm) Coal	A flat, refractory-lined furnace that rotates, carrying the iron ore and carbon mixture through different temperature zones for reduction. Direct reduction occurs in a solid state, with heat supplied predominantly by radiation from overhead burners, facilitating rapid heating and reduction.	Processing low-grade ores or iron-containing by-products. Simple structure of furnace.	Significant levels of impurities, including sulfur. High CO_2 emissions.	≥93%

2.3. DRI Characteristics

Firstly, the characteristics of the feedstock for DRI pellets should be briefly considered. The main characteristics are presented in Table 2, and the iron content should exceed 67% [58,59]. A decreased iron content, leading to a higher proportion of gangue, can create operational challenges in the EAF. These challenges encompass more electricity usage and increased wear on the refractory lining of the furnace, attributed to a rise in slag volume and the transfer of iron to the slag in the form of FeO [60]. Nevertheless, the impact of DRI application in the EAF steelmaking process will be discussed further in Section 6.

Table 2. Characteristics of the main DR pellets, adapted from Refs. [51,58].

Characteristics	Value
Fe_{tot}, wt.%	≥67.0
SiO_2, wt.%	1.0–3.0
Al_2O_3, wt.%	0.2–3.0
MgO, wt.%	0.2–0.9
CaO, wt.%	0.4–1.2
Sulfur, wt.%	≤0.008
Phosphorus, wt.%	≤0.03
Pellet size, mm	9.0–16.0
Porosity, %	~50.0
Compression strength, N	2500–3000
Tumble index, % + 6.15 mm	92.0–95.0
Reducibility index, %	92.0–95.0
Density, $t \cdot m^{-3}$	
bulk	1.6–1.9
apparent	~3.5

Alkali levels should be minimized to prevent swelling and degradation throughout the reduction process. Phosphorus content should be kept to the lowest, below 0.03 wt.%. For DR pellets intended for use in the shaft furnace, sulfur content should be maintained below 0.008 wt.% to avoid clogging the reformer tubes [61].

The quality of DRI (Table 3) is determined by two categories of characteristics: main properties resulting from the DR process, like the metallization degree and carbon content, and inherent properties unrelated to the process, such as gangue content in the raw material. In general, DRI is produced mainly in quality according to the definition by the International Iron Metallics Association [62], characterized by a total iron content ranging between 86.1 and 94.0 wt.% [63] and a metallization degree of 92.0 to 96.0 wt.% [64]. Sulfur content in DRI should be within the range of 0.001–0.03 wt.%, and the phosphorus content should be limited to 0.001–0.09 wt.%. Trace elements like copper, nickel, chromium, molybdenum, and tin are negligible [40].

Table 3. Selected characteristics of DRI, adapted from Refs. [19,62,65–69].

Characteristics	Range, wt.%
Metallization degree	92.0–96.0
Fe_{tot}	86.1–94.0
Fe_{metal}	81.0–89.0
Carbon content	0.02 *–4.5
Sulfur content	0.001–0.03
Phosphorus content	0.001–0.09
Gangue	
Acid	2.5–7.6
Basic	0.5–2.7

* H_2 of the chemical grade was used as a reductant.

DRI predominantly contains silica as the primary gangue component, maintaining an acid gangue composition (mainly SiO_2, Al_2O_3, TiO_2, P_2O_5, Cr_2O_3) and containing basic gangue, for instance, CaO, MgO, MnO, etc. [70,71]. Typically, high levels of gangue elements and inert oxides can diminish the strength of pellets [72]. Oxides, such as SiO_2, Al_2O_3, TiO_2, and V_2O_5, require neutralization through lime additions, influencing both the volume and characteristics of the slag in EAF [73]. The impact of gangue oxides SiO_2, CaO, MnO, and MgO on the reduction process is multifaceted. Although impurities like CaO, MnO, and MgO can lead to swelling and cracking, the right amounts of these gangues could be advantageous. They can create new pathways for the movement of reactants and products, thereby enhancing the rate of reduction reactions [72]. Additionally, according to Tokuda et al. [74], adding SiO_2 to iron oxides significantly reduces their reducibility due to the formation of silicates during the reduction process. This silicate formation leads to low porosity, further decreasing the reducibility of the iron ores. MgO interacts with the intermediate FeO to form (Mg, Fe)O, a compound that presents challenges for reduction [75]. These play a role in prohibiting the reduction process. From the perspective of an EAF, SiO_2 is a surface-active oxide that initially presents a high content in the slag of the hot heel because fluxes are not added until the heat begins. According to Gonzalez et al. [76], this high SiO_2 content can slow the FeO reduction rate. However, this slowing effect can be beneficial as it prolongs the reduction reaction while maintaining an effective, though lower, foam height. As the slag becomes more acidic, the adsorption of SiO_2 at the gas-slag interface intensifies. This reduces the interfacial area available for FeO reduction from the slag.

Table 4 outlines the physical properties of DRI. The density of DRI fluctuates based on its specific form and composition, ranging between 1.5 and 1.9 $t \cdot m^{-3}$ for bulk density and between 3.2 and 3.6 $t \cdot m^{-3}$ for apparent density. The volumetric porosity, however, varies with the production technique and has a mean value of approximately 47.0%. The interaction of DRI with moisture is an important consideration; DRI tends to absorb moisture (12.0–15.0%) from its surroundings, which can lead to oxidation and consequent quality degradation.

Table 4. DRI physical properties, adapted from Refs. [35,58,62,64,77,78].

Characteristics	Value
Bulk density, $t \cdot m^{-3}$	1.5–1.9
Apparent density, $t \cdot m^{-3}$	3.2–3.6
Specific surface area, $m^2 \cdot g^{-1}$	0.5–4.0
Volumetric porosity, vol.%	~47.0
Average size, mm	4.0–20.0
Weight, g	3.0–4.0
Water absorption (saturated), %	12.0–15.0
Fines (−4 mm), %	~5.0

The issue commonly linked to the high specific surface area, porosity, and low density of DRI can often be mitigated through the briquetting process used to produce HBI. This will be detailed in Section 4.3.

3. Carburization

Considering the several advantages of the EAF that are partially associated with the carbon content of DRI [10,79], discussing the carburization phenomenon is relevant. Carburization of DRI during and after the reduction process has various purposes and can be reflected via several reactions, according to Equations (11)–(15):

$$3Fe + CH_4 \rightarrow Fe_3C + 2H_2,\ \Delta H^{\theta}_{298K} = 97\ kJ \cdot mol^{-1}, \quad (11)$$

$$3Fe + 2CO \rightarrow Fe_3C + CO_2,\ \Delta H^{\theta}_{298K} = -150\ kJ \cdot mol^{-1}, \quad (12)$$

$$3Fe + CO + H_2 \leftrightarrow Fe_3C + H_2O,\ \Delta H^{\theta}_{298K} = -108\ kJ \cdot mol^{-1}, \quad (13)$$

$$3FeO + 5CO \leftrightarrow Fe_3C + 4CO_2,\ \Delta H^{\theta}_{298K} = -183\ kJ \cdot mol^{-1}, \quad (14)$$

$$3Fe + C \leftrightarrow Fe_3C,\ \Delta H^{\theta}_{298K} = 23\ kJ \cdot mol^{-1}, \quad (15)$$

The metallization degree, surface area, and porosity [80] influence the DRI carburization rate, along with the presence of active elements in the carburizing gas mixture and the operating temperature and pressure within the DR reactor [68]. The gas reactants are involved in both the reduction and carburization processes concurrently. Since iron ore pellets generally lack carbon-rich components, all the carbon in the DRI can be acquired during the reduction stage. However, this does not apply when H_2 is used as a reductant. DRI carburization is unlikely to occur, which may pose several challenges to EAF melting.

Nonetheless, carbon in the DRI can be presented as bonded carbon: cementite Fe_3C (possible formation of an intermediate carbide Fe_4C before conversion into Fe_3C or Fe_5C_2), a free carbon (graphite), or a combination of both [35]. The carbon of Fe_3C is part of the iron structure, while graphite is not chemically bonded with iron and adheres to the pellet surface or the pore surface, as mentioned in a study by He and Pistorius [81]. However, if this is an issue in the case of DRI, then in the case of using HBI, the graphite present on the surface will be compacted into a dense briquette with a low specific surface area.

The carbon contained in DRI produced, for instance, via a shaft furnace, is usually ≥90% Fe_3C [58]. Fe_3C can decompose at any temperature within the range of 500–900 °C [82]. However, the Fe_3C phase maintains its highest stability at temperatures ranging from 730 to 750 °C. Its decomposition rate accelerates at a temperature decrease from 750 °C and a temperature increase from 770 °C (Figure 2).

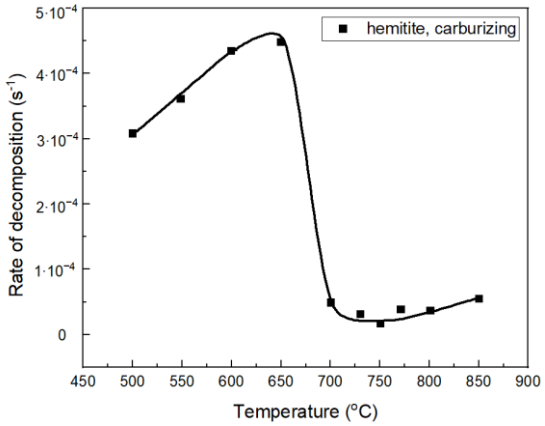

Figure 2. The rate of Fe_3C decomposition depends on temperature, according to a study by Longbottom et al., and is adapted with permission from Ref. [82]. Copyright 2007, Springer Nature.

According to Kumar et al. [83], CO is the main carburization gas, and applying it at 600 °C allows a faster processing rate. Using only CO, or CO with a small amount of H_2, leads to carbon deposition on the surface, particularly at high temperatures, which is undesirable. This is consistent with findings by Olsson et al. [84], who observed that the rate of carbon deposition can increase by up to 70% with H_2 concentration; beyond this point, a higher percentage of H_2 results in a decreased effect. However, adding H_2 to the gas mixture enhances the carburization rate. Ali et al. [22] reported that concentration in the reducing gas mixture enhances the growth of the Fe_3C and carbon deposition up to a certain degree. The highest Fe_3C formation was determined with an H_2:CO ratio of 25:75 at both temperatures of 973 K (~700 °C) and 1059 K (~786 °C), as shown in Figure 3.

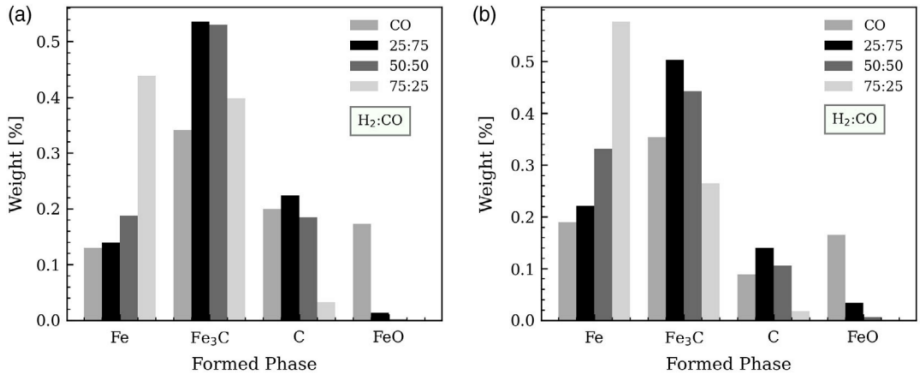

Figure 3. Different phases in the 55% reduced pellets with different gas compositions at: (**a**) 973 K (~700 °C) and (**b**) 1059 K (~786 °C), reprinted from Ref. [22].

In turn, CO_2 reduces the rate at which Fe_3C forms, so its presence in the carburizing gas mixture should be kept to a minimum. Furthermore, gas mixtures primarily composed of CH_4 achieve the fastest carburization rates at temperatures higher than 800 °C. The carburization process and its mechanism are detailed in [85–88].

On the one hand, charging Fe_3C-rich pellets to the EAF compared to graphite-rich pellets can be favorable. The heat formation of Fe_3C is positive, which means that melting of Fe_3C will require lower EAF energy compared to melting a mixture of iron and graphite [68]. Contrary to the abovementioned conclusion, in studies [89,90], it was reported that the DRI pellets, whether they contain graphite or Fe_3C and regardless of the carbon content, show similar melting enthalpies at 1600 °C, melting durations, and initial melting temperatures. This initial melting temperature is approximately 1147 °C, which is near the eutectic temperature for both Fe-Fe_3C and Fe-C systems. A notable difference was found in the melting behavior between graphitic and carbide-containing. DRI samples

with predominantly Fe_3C melted uniformly, while those with graphite carbon displayed localized, spherical liquid areas that slowly developed over time.

Additionally, combining iron with carbon as Fe_3C can associate with the retardation of DRI reoxidation [91]. This advantage can be explained by the lower affinity of Fe_3C for oxygen than metallic iron.

4. Passivation of DRI

4.1. Reoxidation Issue of DRI

In general, removing oxygen from iron ore in the solid state forms numerous microscopic pores, creating a sponge-like texture to the iron [92]. The porosity of the DRI [93] is influenced by the choice of raw materials and the operational conditions prevalent during the DR process. Additionally, variation in reoxidation can be attributed to the differing carbon contents, which the reducing agent determines when used [94]. Therefore, it is important to mention the main mechanisms of reoxidation and the existing methods for mitigating these effects.

Reoxidation can occur via two mechanisms [95]: oxidation in the presence of air atmosphere and corrosion in an aqueous water-based environment. The chemical reactions that lead to the reoxidation of DRI generally release heat, making them exothermic. However, the extent of these reactions can be inhibited due to the carburization phenomenon discussed previously, which offers benefit not only to the EAF but also in terms of hindering reoxidation, owing to the blocking pores [96] resulting from the reduction process and the protective barrier formed by Fe_3C, which shields the material from fast reoxidation.

Dry oxidation progresses gradually at cooler temperatures, whereas the interaction with aqueous water unfolds swiftly and is often the catalyst for higher temperatures to a point where oxidation reactions begin at accelerated rates and turn self-sustaining, caused by rust layers [95]. Initially, reoxidation takes place at lower temperatures due to the exposure of DRI to air, factoring in moisture, according to Equations (16)–(21):

$$2Fe + 2H_2O + O_2 \leftrightarrow 2Fe(OH)_2, \tag{16}$$

$$2Fe(OH)_2 + \frac{1}{2}O_2 \rightarrow 2\gamma\text{—}FeO(OH) + H_2O, \tag{17}$$

$$Fe(OH)_2 + 2\gamma\text{—}FeO(OH) \rightarrow Fe_3O_4 + H_2O, \tag{18}$$

$$2Fe + H_2O + \frac{3}{2}O_2 \leftrightarrow 2FeO(OH), \tag{19}$$

$$3Fe + 4H_2O \leftrightarrow Fe_3O_4 + 4H_2, \tag{20}$$

$$Fe + 2H_2O \leftrightarrow FeO(OH) + \frac{3}{2}H_2, \tag{21}$$

Reactions (22)–(24) are highly exothermic, releasing a level of heat sufficient to boost additional oxidation processes:

$$3Fe + 2O_2 \leftrightarrow Fe_3O_4, \tag{22}$$

$$2Fe_3O_4 + \frac{1}{2}O_2 \leftrightarrow 3Fe_2O_3, \tag{23}$$

$$Fe + \frac{1}{2}O_2 \leftrightarrow FeO, \tag{24}$$

Implementing an inertization [97] or passivation technique enhances the stability of DRI for secure handling, transport, and storage. Various technologies exist for DRI passivation, as shown in Figure 4, each presenting its own set of advantages and disadvantages. However, none match the relatively higher efficiency of hot briquetting.

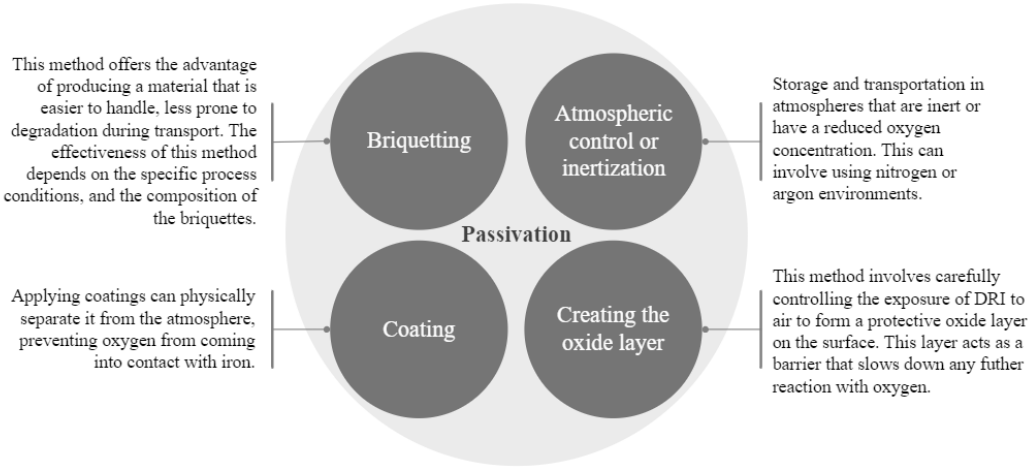

Figure 4. Main passivation techniques for DRI.

4.2. Creating the Oxide Layer

DRI can be maintained in an environment containing minimal oxygen to prevent reoxidation and create a thin oxide layer over all exposed surfaces. The reoxidation rate of DRI depends significantly on the morphological structure [98]. The morphological structure of DRI depends on the chemical composition of the iron ore, physicochemical properties of the pellets, reduction temperature, and gas compositions. If the time interval between reduction and oxidation is short, the reoxidation rate of DRI under air can be high. According to studies [95,99], the reoxidation process of iron initially does not maintain a constant temperature due to its exothermic nature, which heats the iron further. This process unfolds in three stages: the first phase shows quick oxidation, and the surface chemical reactions dominate; the second phase sees a gradual slowdown in oxidation, and the process indicates internal diffusion; the third phase has a low and stable oxidation rate, limited by slow diffusion, with a potential slight increase if the temperature rises. In conclusion, diffusion within the iron and forming cavities at the interface between the oxide layer and iron grains become the key mechanisms.

Abd Elmomen [94] oxidized reduced single DRI pellets in ambient air at an average temperature of 27 °C. The reaction duration varied from 1 to 50 days. The degree of reoxidation was determined by weight gain over time and the mass balance method. The reoxidation process proceeded topochemical and was controlled by the apparent rate of chemical reaction at the interface between the oxide layer and the unreacted core of metallic iron. It was concluded that the increase in the reoxidation degree and the accompanying decrease in the metallization degree depended on the source of oxide pellets used for DRI production.

In another study by Abd Elmomen [100], the kinetics of DRI reoxidation under stagnant air at temperatures between 150 and 450 °C were studied using two series of experiments. The first is in the relatively low-temperature range between 150 and 250 °C, and the second is at higher temperatures from 300 to 450 °C. In the mentioned low-temperature range, the reoxidation process was governed by a chemical reaction at the gas-unreacted core. No significant reoxidation occurred below 200 °C. In the relatively higher temperature range (300–450 °C), the reoxidation process proved to be controlled by pore diffusion.

Upadhya [101] also reported that below 220 °C, no significant reoxidation was observed. Additionally, it was found that the reoxidation rate became independent of the airflow above a critical flow rate of 0.85 L·min^{-1}, indicating that at this stage, the influence of the gas boundary layer around the DRI pellet becomes negligible. The auto-ignition temperature of these DRI pellets was within the range of 200–230 °C.

Medina [102] reported that the reoxidation rate under dry air increased with increasing test temperatures to a maximum of 400–500 °C. In contrast, further increases in the test temperature reduced the rate of DRI reoxidation.

For pellets, after reduction in a hydrogen atmosphere, in the study by Cavaliere et al. [95], a very slow weight increase for temperatures up to 500 °C under air due to reoxidation was observed. Further, reoxidation occurred more rapidly at higher temperatures, with a weight increase of 4% after 10 min of exposure to 700 °C under air.

Moreover, there is a difference in reoxidation behavior between gas-based and coal-based DRI. In a moist oxygen-containing atmosphere, the activation energy for high-carbon gas-based DRI can be around 55 kJ·mol^{-1} (non-isothermal, heating rate of 15 °C·min^{-1}), and activation energy for coal-based DRI can be around 20–35 kJ·mol^{-1} (non-isothermal, heating rate of 15 °C·min^{-1}) [103,104]. Moreover, Bandopadhyay et al. [103] concluded that the gas-based DRI oxidizes relatively more quickly at approximately 447 °C, but at temperatures above 527 °C, the oxidation rate slows down, presumably because of the simultaneous oxidation of carbon.

4.3. Hot Briquetted Iron

Combining a high specific surface area and a porous structure in DRI increases susceptibility to reoxidation reactions [105]. The HBI was created in response to the issues with the shipping of DRI noted above, along with the need to briquette the fine metallic iron produced in the fluidized bed reduction processes [58] and pellets or lump ore from shaft furnace processes [16]. HBI is the compressed and densified version of DRI [106]. The material should be at a temperature of 650–700 °C before being compressed between two rollers. This process forms briquettes that typically measure between 90 and 140 mm in length, 48–58 mm in width, and 20–50 mm in thickness [107,108] and show a bulk density of 2.4–3.3 t·m^{-3} and an apparent density of 5.0–5.5 t·m^{-3} (Table 5). The variation in chemical and physical properties between DRI and HBI branches from the production pathways they undergo. Factors such as the grade and blend of the used ore, the nature of gangue materials, metallization degree, the use of additives, and the briquetting conditions also contribute to this variation.

Table 5. HBI physical properties, adapted from Refs. [35,58,64,77,78,108].

Characteristics	HBI
Bulk density, t·m^{-3}	2.4–3.3
Apparent density, t·m^{-3}	5.0–5.5
Specific surface area, m^2·g^{-1}	~0.75
Volumetric porosity, %	~21.0
Weight, g	500.0–700.0
Water absorption (saturated), %	~3.0
Fines (−4 mm), %	1.0–3.0

Compared to DRI, HBI has higher density and lower porosity. Due to its lower porosity, HBI tends to absorb less environmental moisture. In addition, HBI exhibits better wear and corrosion resistance due to its high bulk density, decreasing reactivity by one to two orders of magnitude [51,109].

HBI may undergo partial oxidation during handling, transportation, and storage processes, reducing its metallization degree. Environmental factors, along with production and briquetting parameters like the type of ore being reduced, as well as the pressure and temperature used during briquetting, significantly impact the rate of reoxidation. These variables influence the density of the briquettes, thereby affecting their reoxidation behavior, which can lead to the creation of various phases (Figure 5), for instance, ferrous hydroxide ($Fe(OH)_2$) [110], ferrous oxide (FeO), etc. Additionally, corrosion products can be detected as lepidocrocite (γ-FeO(OH)), iron trihydroxide ($Fe(OH)_3$), magnetite (Fe_3O_4), goethite (γ-FeO(OH)), maghemite (γ-Fe_2O_3), etc. [111].

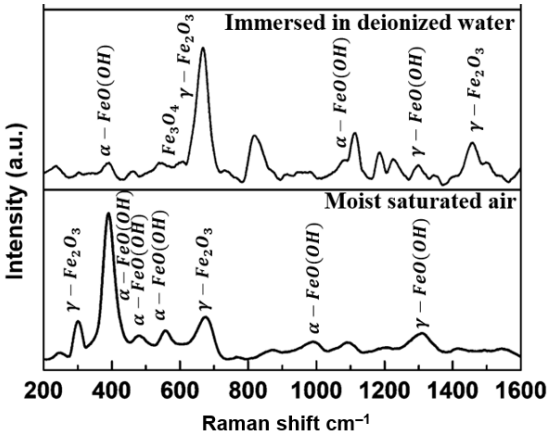

Figure 5. Raman spectra of possible phases can be detected in reoxidized HBI under different conditions, adapted from Ref. [109].

In this regard, Daghagheleh et al. [109] tested HBI samples under five different prepared climatic conditions for four months. Depending on the condition, different oxidation behaviors were observed. The results are shown in Figure 6 for both wet and dried HBI samples and the calculated metallization loss based on chemical analysis. HBI samples, which were exposed to ambient air conditions, developed nearly no reoxidation. The reoxidation was raised when the HBI samples were exposed to moisture-saturated air conditions. The reoxidation was further accelerated if the HBI samples were immersed constantly in deionized water. Immersing in process water has accelerated the reoxidation further. The worst case was experienced by samples periodically immersed in process water twice a week, each time for 1h comparison. The final metallization loss values were 0.92, 3.24, 4.26, 5.57, and 6.96 wt.% under ambient air, moist saturated air, immersed in deionized water, immersed in process water, and periodically immersed in process water, respectively. The porosity of the most reoxidized HBI samples was smaller than the raw HBI. The closure of cracks and pores by reoxidation products resulted in low porosity. The physical strength of the samples showed no significant difference before and after the reoxidation experiment. It can be concluded that interval and cyclic wetting and drying of HBI leads to the worst metallization loss problem. This case should be avoided from handling, storage, and shipment aspects.

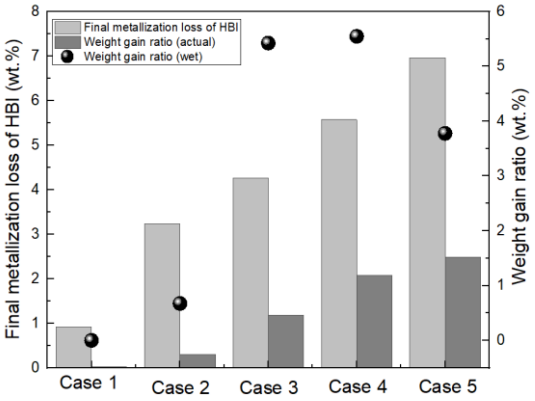

Figure 6. The final metallization loss of the dried HBI and weight gain ratio before and after drying were plotted based on data from Ref. [109].

The conditions under which the DRI was produced significantly influenced the reoxidation resistance of briquettes when exposed to oxidizing conditions [112,113].

From a laboratory-scale perspective, Gray et al. [114] reported that HBI derived from DRI with a 1.5 wt.% carbon content (produced at reducing temperatures between 500

and 800 °C, using a reducing gas composition of 70–75% H_2 and CO, along with H_2O, CO_2, CH_4, and N_2) showed more corrosion resistance compared to HBI from DRI with a 0.053 wt.% carbon content (produced at a reducing temperature of 630 °C with 100% H_2). This difference in performance is attributed to the variations in chemical compositions resulting from different reducing gas mixtures and ore types. Additionally, it was noted that briquettes with higher density (produced at 600 °C with a density of 5.2 g·cm^{-3}) demonstrated better corrosion resistance than those with lower density (produced at 500 °C with a density of 4.2 g·cm^{-3}).

Practically, there is a notable gap in understanding the reoxidation process, particularly with HBI, and measurements that should be considered subsequently for handling and transportation. In this context, the currently running HBI-C-Flex project is funded within the frame of the Research Fund for Coal and Steel (RFCS, Grant Agreement no. 101112479) [115] gains significance as it aims to test the reoxidation of HBI and DRI (with different carbon contents and low-grade iron ore application) under varying environmental conditions (including both dry and wet atmospheres and higher temperatures) to measure the exothermic reactions that occur during storage and transportation. Insights into the reactivity and stability of HBI, including dust formation, will be crucial for steel manufacturers. Further investigation will aid in improving logistics and enhancing knowledge to prevent dangerous situations in operations.

4.4. Other Methods

Applying coatings to DRI [51], such as sodium silicate, limestone, cement, or waxes [116,117], is a potential strategy for retardation of reoxidation. However, the disadvantages of coatings include the risk of additional contamination, increased costs, and the possibility of the coating being scratched during handling and transportation. Another disadvantage that can be considered is that coated DRI pellets can consume more electricity and graphite electrodes in the EAF compared to uncoated DRI pellets [118]. Nevertheless, to evaluate the effectiveness of the waxing process in preventing reoxidation of DRI, as detailed in [119], the experiment was conducted where the DRI was immersed in a bath of melted paraffin at temperatures between 110 and 120 °C for 3–5 s. It was observed that no heat was produced from the treated DRI after it was sprayed with a 5% sodium chloride solution, suggesting that corrosion did not occur. Additionally, there was no change in weight after the DRI was heated to 150 °C for 30 min in an air jet oven, indicating the absence of reoxidation and no loss of wax. Furthermore, no dust was released from the treated DRI samples following a tumbler index test.

After ammonia DR [120–124], it was noticed that the nitride passivates the otherwise highly active reduced iron, offering a safety-critical benefit for handling and logistics. Nitride formation presents a benefit of the ammonia DR process, as it enhances the aqueous corrosion resistance of iron. Specifically, during the quenching process (at temperatures below 700 °C), metallic iron within the sample undergoes nitriding in the presence of NH_3. Conversely, in the absence of NH_3 at 700 °C, nitrides decompose back into metallic iron. This indicates that the quenching conditions are crucial in determining the phases produced. Consequently, the phases present in the reduced ore can be effectively managed during the post-reduction stage [120].

Several factors, including the origin and type of iron ore, affect the stability, reactivity, and reducibility of DRI. Improving the resistance of DRI to reoxidation and spontaneous ignition involves prolonging the reduction process and increasing its temperature. The gas composition during DR impacts the quality of reduction and carbide stability, while the porosity of DRI increases its reoxidation occurrence. As mentioned above, briquetting DRI into HBI reduces its specific surface area and exposure to air, enhancing stability by forming a protective layer against further reoxidation.

5. Storage, Handling, and Transportation

Some main measurements can be extracted from [35,125–127] and generalized as follows. For safe DRI storage, it is critical to avoid storing any DRI hotter than 65 °C in bins or silos, instead keeping it isolated and not stacked higher than one meter. Safety measures include conducting regular gas analyses to keep oxygen below 3% and detecting hydrogen production. Monitoring and managing temperatures within storage units are essential, with procedures to seal and ventilate units if temperatures reach 65–75 °C. During extended storage, introducing inert gas prevents reoxidation, and ensuring slide gates remain closed maintains a stable, safe environment.

Additionally, according to [128], DRI can be categorized into three types: less reactive (category A), namely HBI; highly reactive (category B); and by-product fines (category C), which are generated after production and handling of DRI or HBI. Depending on the category, particular recommendations for loading and carriage are described in detail [127].

6. Application of DRI/HBI in an EAF Steelmaking

Process-wise, in DRI-based steelmaking, there are two primary methods for sourcing. The first method involves directly melting the DRI as soon as it exits the DRI production process. Alternatively, the second method utilizes HBI, which is cold, compacted, and treated for safe transportation. This approach offers flexibility by separating the DRI production process from steelmaking, allowing for more logistical and operational convenience [129]. HBI and hot DRI possess similar advantageous characteristics to those of cold DRI. However, for hot DRI, its temperature plays a crucial role in enhancing EAF efficiency while maintaining its high metallic content [130,131]. Hot DRI can be transported to an EAF at a temperature of ~700 °C [132] using various methods, including hot transport vessels, pneumatic transport systems, hot conveyors, and gravity systems [51,133]. This approach can lower electrical energy usage, leading to energy savings of approximately 20–30% [132] compared to traditional furnaces that are fed with cold materials. Additionally, according to Gonzalez et al. [134], as the initial temperature of the DRI increases, the melting rate augments; thus, tap-to-tap time decreases, promoting higher productivity. The full potential of this hot charging technology is not completely leveraged due to the differing operational requirements between EAF and DRI production processes [132]. Nevertheless, using hot DRI charging offers some benefits [134,135].

Typically, DRI/HBI can be charged with scrap in varying amounts to the EAF, influenced by local cost factors and material availability [19]. DRI/HBI can be within the range of 10–30% of the total charge [133] in the EAF. HBI, often added to the EAF alongside scrap using buckets, requires minimal adjustments to the existing EAF, mainly when HBI constitutes up to 10% of the charge. The design of the EAF can allow for an increased "hot heel" or the remaining melt volume, which can be up to 30% [136] of the total melt volume. This adjustment aids in the effective melting of DRI. Consequently, to accommodate the continuous addition of materials, maintain prolonged periods of a flat bath, and manage the increased need for lime and calcined dolomite for slag formation, adjustments to the power programs of the EAF are necessary.

In EAF, DRI/HBI demonstrates different characteristics than the steel scrap melting. This variation can be based on DRI/HBI/scrap share, metallization degree [137], and due to gangue and carbon within the DRI/HBI [138]. Since the DR process operates in a solid state, the gangue from the DR pellets is not removed but instead transferred into the EAF along with the DRI. This results in increased amounts of slag during the steelmaking process due to the higher levels of gangue content [139].

As the DRI/scrap ratio increases and the DRI metallization degree decreases, the iron oxide content in slag can increase. An increase in the SiO_2 content in DRI demands a higher CaO addition to keep the basicity ratio, subsequently increasing energy demands [77]. According to Kirschen et al. [19], the average iron loss in EAF using DRI can be greater than in using scrap, and controlling FeO content proves more challenging in EAF with DRI.

The standard deviation of FeO ranged from 3.9 to 5.5 for scrap and widened from 4.1 to 9.6 when the DRI usage was >50% (Figure 7).

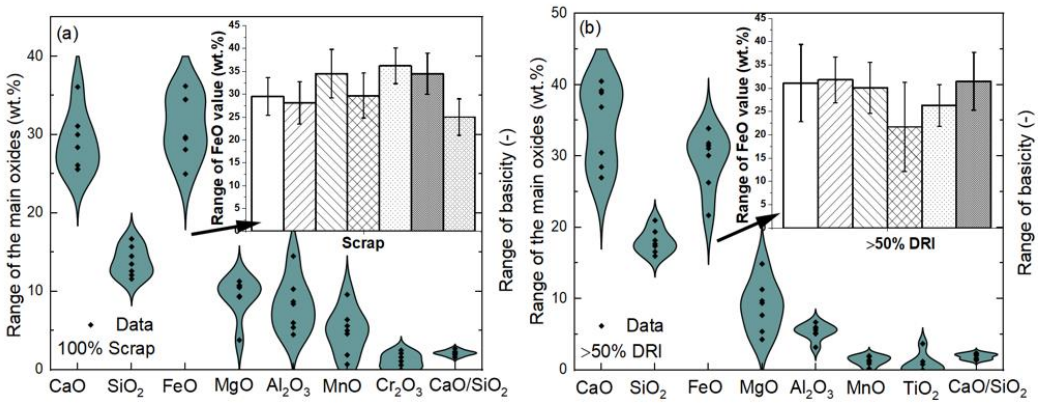

Figure 7. Range of main oxides in EAF slag depending on charged material: (**a**) 100% scrap; (**b**) >50% DRI, plotted based on data from Ref. [19].

Additionally, the yield from DRI inputs can be typically lower, which is attributed to the oxide gangue content in DRI. This contrasts with the yields from melting 100% scrap, which range from 90 to 94% (Table 6). The melting time and tap-to-tap time for DRI-based production are considerably longer than those used for scrap [19].

Table 6. Production parameters of EAF charge with scrap and scrap/DRI for low alloyed steel grades, adapted from Refs. [16,19].

Production Parameters	100% Scrap	80–95% DRI
Share of DRI/HBI, % procedures	0–5 (HBI)	60–95 (DRI)
Electric energy demand, kWh·t^{-1}	310–460	530–680
Natural gas, m^3·t^{-1}	3–10	0–2
Oxygen, m^3·t^{-1}	25–40	20–35
Coal and carbon fines, kg·t^{-1}	2–9	8–17
Slag former, kg·t^{-1}	23–35	27–60
Tap temperature, °C	1600–1635	1600–1635
Tap-to-tap time, min	50–60	60–100
Metal yield, %	90–94	87–92

Concerning carbon in DRI, it serves several reasons [10,79]: first, carbon is essential for the complete metallization of iron; second, it serves as an additional energy source. When oxygen is injected to burn the carbon, it reduces the need for electricity, thereby accelerating the melting process of the materials charged. Third, carbon is necessary to create a foamy slag in the EAF, benefiting the process (Figure 8). For instance, for each 1.0 wt.% of iron in the form of FeO within the DRI, theoretically, 0.215 wt.% of carbon is needed to reduce it through the endothermic reaction FeO + C → Fe + CO [35]. Furthermore, carbon can be engaged in various oxidation reactions with CO formation, such as $CO_2 + C \rightarrow 2CO$ ($\Delta H \geq 0$) and $C + \frac{1}{2}O_2 \rightarrow CO$ ($\Delta H \leq 0$), which can facilitate stirring. Different from carbon materials that are charged or injected [140–142], DRI contains carbon but is free from volatile matter, ash, and sulfur, which can affect the melting process and/or the quality of steel.

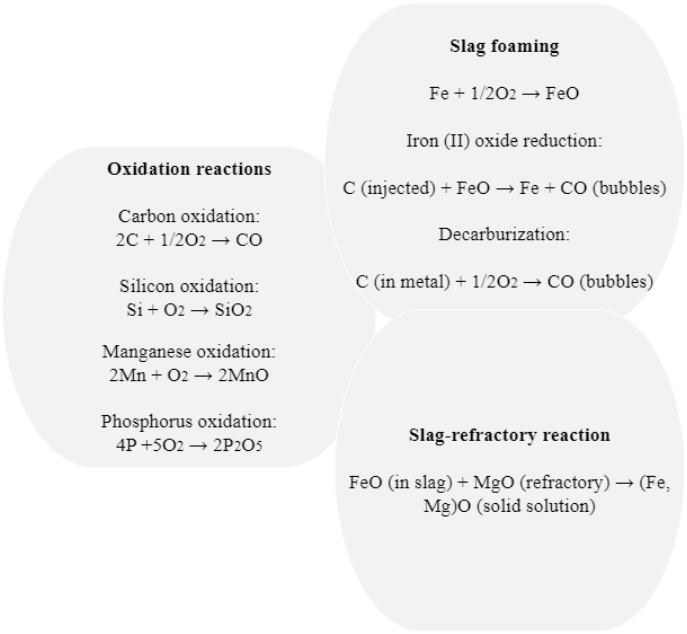

Figure 8. Chemical reactions in an electric arc furnace, adapted from Ref. [143].

According to Memoli et al. [144] DRI is more effective than charged carbon material in the bath reactions, yields, and purity of the carbon in the steel.

Lule et al. [145] highlighted results from the ArcelorMittal Lázaro Cardenas steelmaking shop, focusing on N_2 behavior. The use of high-carbon and a high proportion of DRI proved advantageous for producing N_2-critical steel grades, attributed to the significant evolution of CO bubbles allowing the N_2 transfer from the liquid steel to the gas atmosphere in the bubble. The same behavior was also claimed by Memoli et al. [144].

Several studies have also been devoted to investigating the influence of the DRI amount on the steelmaking process parameters. With increasing the percentage of DRI in the charge, there can be a noticeable decrease in metallic yield, tramp elements, and sulfur, as reported in [146]. Similar observations of improvement in steel quality by increasing the DRI percentage (varying range of DRI of 0–90%) have been noticed by Elkader et al. [66]. The reduction in tramp (copper, tin, nickel, and chromium), phosphorus, sulfur, and nitrogen were correlated with increased DRI proportions. Conversely, a rise in the DRI content resulted in greater per-ton consumption of electric power, oxygen, coke, and fluxing agents required to produce liquid steel. Additionally, as the percentage of DRI in the charge increased, there was an extension in both power-on and overall tap-to-tap times.

Hassan et al. [147] studied the impact of DRI/HBI on the steelmaking process parameters (Figure 9a,b), along with methods and proportions (case 1: 100% steel scrap; case 2: 100% HBI in the proportion of metallic charge of 17.36%; case 3: 100% HBI in the proportion of metallic charge of 26.76%; case 4: 50% HBI: 50% DRI in the proportion of metallic charge of 45.16%; case 5: 100% DRI in the proportion of metallic charge of 75.02%; and case 6: 100% DRI in the proportion of metallic charge of 100% of DRI) under the temperature condition of 1640 ± 10 °C. Increasing the amount of lower-quality DRI and/or HBI to 45% of the metallic charge decreased steel yield to 85.32%. Conversely, the yield increased to 87.57% when the input consisted of 75–100% high-quality DRI, continuously fed. This led to a 21-min decrease in tap-to-tap time and a 7% decrease in electrode usage. Increasing the proportion of lower-quality DRI in the EAF from 45% to 100% resulted in a 4 tons/heat decrease in liquid steel and caused lime usage to increase from 4 to 6 kg·t_{LS}^{-1}.

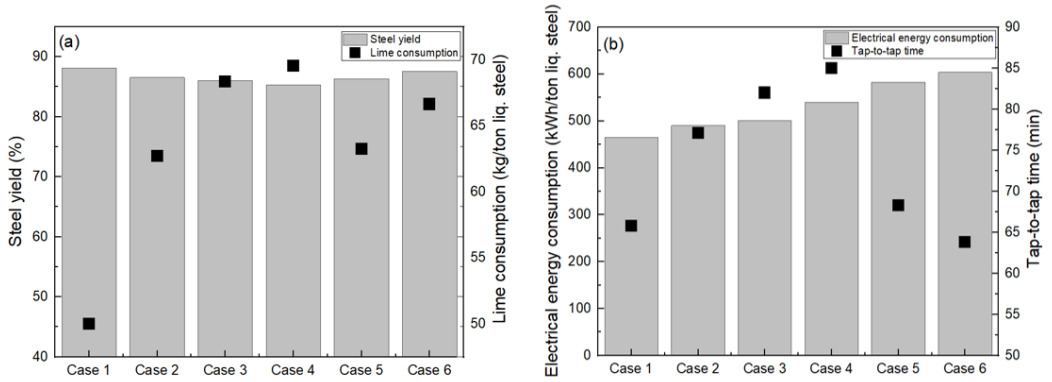

Figure 9. Impact of DRI/HBI on the selected steelmaking process parameters: (**a**) steel yield and lime consumption; (**b**) electrical energy consumption and tap-to-tap time, plotted based on data from Ref. [147].

The use of DRI can affect refractory degradation by altering the composition of slag, specifically reducing the CaO/SiO_2 basicity [148]. Heo and Park [149] investigated the interfacial reactions between the EAF slag of 20 wt.% CaO—16.9 wt.% SiO_2—39.6 wt.% FeO—3.2 wt.% MgO—13.1 wt.% Al_2O_3—7.2 wt.% MnO and magnesia refractory, varying the addition of DRI (0, 10, 20, 30 wt.%). Their investigations were conducted at 1550 °C under an argon atmosphere. They suggested that controlling the amount of DRI is essential to reduce refractory degradation during the EAF process, as increasing DRI content can decrease the CaO/SiO_2. Further, Heo and Park [150] conducted research on how temperature variations between 1550 and 1650 °C impact the chemical interaction at the boundary between the slag, composed of CaO—SiO_2—MgO—35 wt.% FeO—10 wt.% Al_2O_3—5 wt.% MnO, and the refractory under conditions incorporating 20 wt.% DRI in the EAF. Their findings suggest that precise temperature control in an EAF process that utilizes DRI plays a more crucial role in reducing refractory wear than the proportion of DRI used.

Furthermore, DRI melting in the EAF process encompasses heat, mass, and momentum transfer, as well as a multiphase system comprising liquid slag, liquid steel, evolving gases, and solid particles [134]. As mentioned above, the physical properties and chemical composition of DR influence the melting process. Factors such as the method of charging, furnace type, bath temperature, the chemical composition of the molten phases, and the circulation of fluids within the furnace and around the particles should also be considered.

Understanding how DRI behaves when immersed in liquid slag is based on several research data obtained under a laboratory scale, which will be discussed further and tends to be more about qualitative or visual descriptions of experiments rather than quantitative results. Based on visual observations of the DRI behavior in liquid slag, it can be categorized as follows: sink through, float inside the slag, or remain on top before complete decarburization.

The study by Li and Barati [132] is one of the most thorough in explaining the behavior of DRI in slag. To understand the decarburization and melting behavior of DRI pellets, the SiO_2-Al_2O_3-CaO-MgO slag with various FeO contents (10–25 wt.%) and basicity $(MgO + CaO)/(SiO_2 + Al_2O_3)$, ranging from 1.5 to 2.5, has been used. The result showed that the decarburization of DRI in slag at 1600 °C takes place in two stages: initially, the reaction is between FeO and the carbon within the pellet, driven by heat transfer from the slag to the pellet. The subsequent phase involves FeO from the slag reacting with the remaining carbon in the DRI. The reaction rate depends on how FeO moves within the slag and is heavily influenced by its concentration. Additionally, in the study, three possible behaviors of DRI were observed in slag. In the first case, the DRI pellet immediately sinks to the bottom of the crucible, creating a thin and uneven gas layer that occasionally moves the pellet. This was attributed to the weaker gas evolution of $8.35 \cdot 10^{-5}$ $mol \cdot s^{-1}$ in the first stage of decarburization. In the second case, the DRI pellet stays buoyant and moves within the slag due to a thicker gas halo forming around it until it turns into a liquid droplet and

sinks. In the third case, high slag viscosity causes the pellet to partially immerse and restrict its movement, linked to a higher gas-evolution rate of $2.11 \cdot 10^{-4}$ mol·s^{-1} in the first stage of decarburization. In all cases, it was observed that the pellet began to shrink after 16–26 s of immersion, and a dense shell was formed around the pellet.

It should be mentioned that firstly, Mulholland et al. [151] observed the gas layer in their research on the reaction between iron-carbon-sulfur drops (0.8–4.5 wt.% C, 0.04–1.0 wt.% S) and steelmaking slag (47 wt.% CaO—38 wt.% SiO_2—15 wt.% Al_2O_3—10–30 wt.% Fe_2O_3) via X-ray technique at 1723–1873 K (approximately at 1450–1600 °C). It was concluded that the Fe-C-S drop into the slag initially floats, followed by slag foaming. Subsequently, the drop sank, and the foamy slag layer disappeared. Notably, it was impossible to determine the different velocities of the drop's movement to the bottom of the crucible, which varied widely, ranging within 1–36 cm·s^{-1}. According to Min and Fruehan [152], the reaction apparently occurs in two steps: one at the gas slag interface and the other at the gas metal interface, with CO_2 diffusion through the gas halo.

A similar manner was reported by Goldstein et al. [153] when studying the behavior of cold DRI pellets dropped into a slag system of 40 wt.% CaO—41 wt.% SiO_2—10 wt.% Al_2O_3—9 wt.% FeO at 1460 °C. The gas rate produced from the FeO reduction in the DRI was measured by a constant volume pressure increase method. It indicated a short incubation period of approximately 2–4 s, followed by rapid gas evolution from the pellet that lasted between 20 and 30 s. The gas halo formed around the pellet, causing the pellet to remain buoyant in the slag.

From the point of view of the dependence of melting time on several physical properties of DRI, Gonzalez et al. [134] suggested that the melting time is significantly affected by the thermal conductivity of DRI. They noted that increasing the metallization degree of DRI and reducing its porosity can raise thermal conductivity. Additionally, it was highlighted that an increase in porosity adversely affects melting time, leading to longer durations for the melting process.

Sharifi et al. [154] investigated how the initial carbon content and the preheating temperature of DRI affect the reaction rate, aiming for a slag composition of 22 wt.% FeO—42 wt.% CaO—22 wt.% SiO_2—4 wt.% Al_2O_3—10 wt.% MgO, with temperatures ranging from 1500 to 1600 °C. They determined that the decarburization of DRI could occur in two distinct stages. Furthermore, preheating DRI pellets was found to accelerate the initiation of the reaction between carbon and FeO, thus shortening the total reaction time (Figure 10). This reduction suggests a potential for enhancing the productivity of DRI-based steel production through the preheating of DRI.

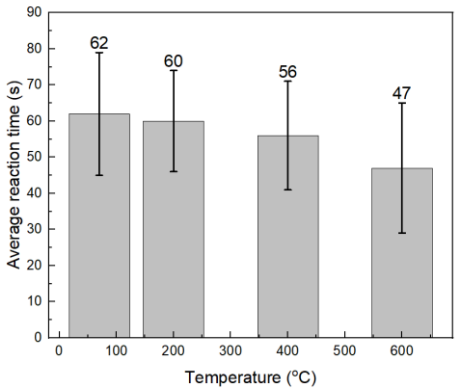

Figure 10. Average reaction times for four preheating temperatures of DRI, plotted based on data from Ref. [154].

Considering the conclusion of the study by Sharifi et al. [154] that the decarburization of DRI pellets takes place in two stages: a reaction between FeO and carbon inside the pellet, followed by a reaction of the remaining carbon with the FeO inside the slag, Kiasaraei [155] reported that the duration of each stage varies based on the carbon and FeO levels in the

DRI, with the second stage potentially being negligible in cases of low carbon content. The study highlights the significant impact of carbon content on decarburization rates, noting an increase in reaction rate for both phases with higher carbon levels, especially in the second stage. Additionally, it was determined that heat transfer mechanisms predominantly control the reaction rate in the first stage, indicating its role as an important factor. Li and Barati came to the same conclusion [132].

Furthermore, research was conducted on how the size of DRI pellets influences the process, and different conclusions were reported [153,156]. Sadrnezhaad [157] stated that the optimum size of the DRI pellets was around 7 mm for experiments. The optimum feeding rate for the lowest energy consumption was 12.5 $g \cdot s^{-1}$ for continuous feeding of DRI for a 25 kg induction furnace at 1550 °C. In addition, it was determined that a DRI pellet with a metallization degree of 92.5% and carbon content of 1.6 wt.% could be assumed to behave like an isolated gassing particle floating on the surface of the liquid melt. The heating and melting process took a few seconds compared to the case with the highly metalized DRI of 97%.

A notable reduction in melting rate can be observed for DRI particles with large sizes, for instance, above 10 mm, according to González et al. [134], and when the arc length is elevated [21]. However, with an increase in the initial particle size, the thickness of the frozen shell, which plays a large role in the melting rate of DRI, can rise. In addition, extended arc operation can harm the refractory of a furnace by creating intense hot spots and reducing thermal efficiency through uncontrolled radiation. This issue can be mitigated by employing foamy slag.

The productivity of an EAF that continuously melts DRI depends on the chemical composition of DRI, the feed rate of the DRI, and effective slag foaming. The yield of liquid steel when using DRI or HBI depends on the metallization degree, the total content of gangue, and carbon injection. In general, achieving a higher yield of liquid steel requires a greater degree of metallization in DRI or HBI.

7. Conclusions and Prospects

The DR-EAF route presents an alternative to the conventional BF-BOF route. The production route of DRI can be divided into one that uses gas reductants (converted NG, syngas, H_2, etc.) and another that relies on coal. Investigating various H_2-containing reducing gases and their combinations can be relevant. In this regard, exploring alternative H_2 carriers like ammonia is viable, along with the potential to not only be a source of the required H_2 but also provide a solution against reoxidation.

In the case of DRI carburization, when carbon or carbon-containing gases (CO/CH_4) are applied to facilitate effective carburization, it is important that the gas mixture used minimizes CO_2 and optimizes the ratio of CO to H_2. The presence of CH_4 in the gas mixture can also accelerate the carburization process at temperatures above 800 °C. Alongside this, the presence of carbon in DRI from the perspective of EAF can have some benefits than charged/injected carbon material.

Concerning reoxidation behavior, and based on the research results, several general conclusions can be drawn. Significant reoxidation is usually not observed at low temperatures under air. However, in some cases, further reoxidation can occur more rapidly at higher temperatures, up to 700 °C under air conditions. The reoxidation process can be accompanied by a degree of loss of metallization. As mentioned earlier, the briquetting of DRI is one of the most efficient methods to prevent reoxidation. However, the pre-conditions and environmental factors can influence the reoxidation behavior of HBI. Further research on the reoxidation behavior of HBI could enhance understanding of its reoxidation mechanisms and enable the development of more effective mitigation strategies for handling and transportation. This is particularly important as most existing studies have primarily concentrated on the reoxidation of DRI rather than HBI. The analysis presented did not fully explore the reoxidation behavior of DRI/HBI produced using H_2 as a reducing agent due to a scarcity of such findings in the existing literature. This gap highlights the potential

value of research in this area, particularly regarding the establishment of handling and transportation conditions.

Considering the possibility of further research prospects in terms of processing low-quality iron ore with high gangue content, the DR-EAF route is advantageous for processing high-quality iron ore (≥67% Fe), allowing flexible supplementation of DRI and HBI with scrap based on market conditions. However, the availability of high-grade ores is limited. In contrast, from the point of view of prospects, the DR-electric smelting furnace-BOF route is more suitable for processing low-quality iron ore with high gangue content. This route involves further refining the pre-melt in a conventional BOF and offers the additional benefit of using smelter slag in the cement industry.

Author Contributions: Conceptualization, L.K., S.L. and O.D.; methodology, L.K., S.L. and O.D.; resources, J.R.; data curation, L.K., S.L. and O.D.; writing—original draft preparation, L.K.; writing—review and editing, L.K., S.L., J.R., M.L., L.S. and O.D.; project administration, L.S. and M.L. All authors have read and agreed to the published version of the manuscript.

Funding: This research receives funding from the European Union (RFCS Research Fund for Coal and Steel) within the frame of the "HBI C-Flex" project, Grant Agreement number 101112479.

Data Availability Statement: The raw data supporting the conclusions of this article will be made available by the authors on request.

Acknowledgments: This research work is related to the "HBI C-Flex" project and receives funding from the European Union (Research Fund for Coal and Steel) under grant agreement No 101112479. Furthermore, the authors gratefully acknowledge the funding support of K1-MET GmbH, a metallurgical competence center. The research program of the K1-MET competence center is supported by COMET (Competence Center for Excellent Technologies), the Austrian program for competence centers. COMET is funded by the Federal Ministry for Climate Action, Environment, Energy, Mobility, Innovation, and Technology, the Federal Ministry for Labour and Economy, the Federal States of Upper Austria, Tyrol, and Styria, as well as the Styrian Business Promotion Agency (SFG) and the Standortagentur Tyrol. Furthermore, Upper Austrian Research GmbH continuously supports K1-MET. Besides the public funding from COMET, this research project is partially financed by scientific and industrial partners.

Conflicts of Interest: Authors Lina Kieush, Stefanie Lesiak, Johannes Rieger, Melanie Leitner, Lukas Schmidt were employed by the company K1-MET GmbH. The remaining authors declare that the research was conducted in the absence of any commercial or financial relationships that could be construed as a potential conflict of interest.

References

1. Dall'Osto, G.; Mombelli, D.; Mapelli, C. Consequences of the Direct Reduction and Electric Steelmaking Grid Creation on the Italian Steel Sector. *Metals* **2024**, *14*, 311. [CrossRef]
2. Pfeiffer, A. Evaluation of the Smelting Behaviour of Direct Reduced Iron. Ph.D. thesis, Montanuniversitaet Leoben, Leoben, Austria, 2023.
3. Béchara, R.; Hamadeh, H.; Mirgaux, O.; Patisson, F. Optimization of the Iron Ore Direct Reduction Process through Multiscale Process Modeling. *Materials* **2018**, *11*, 1094. [CrossRef]
4. Fei, Y.; Guan, X.; Kuang, S.; Yu, A.; Yang, N. A Review on the Modeling and Simulation of Shaft Furnace Hydrogen Metallurgy: A Chemical Engineering Perspective. *ACS Eng. Au* **2023**, *4*, 145–165. [CrossRef]
5. Diez, M.A.; Centeno, T.A.; Amado-Fierro, Á. Coal Use for Iron and Steel Production in Low-Carbon Transition Scenarios. In *The Coal Handbook*; Elsevier: Amsterdam, The Netherlands, 2023; pp. 493–546, ISBN 978-0-12-824327-5.
6. Hammam, A.; Cao, Y.; El-Geassy, A.-H.A.; El-Sadek, M.H.; Li, Y.; Wei, H.; Omran, M.; Yu, Y. Non-Isothermal Reduction Kinetics of Iron Ore Fines with Carbon-Bearing Materials. *Metals* **2021**, *11*, 1137. [CrossRef]
7. Boretti, A. The Perspective of Hydrogen Direct Reduction of Iron. *J. Clean. Prod.* **2023**, *429*, 139585. [CrossRef]
8. Devlin, A.; Kossen, J.; Goldie-Jones, H.; Yang, A. Global Green Hydrogen-Based Steel Opportunities Surrounding High Quality Renewable Energy and Iron Ore Deposits. *Nat. Commun.* **2023**, *14*, 2578. [CrossRef]
9. Ling, J.; Yang, H.; Tian, G.; Cheng, J.; Wang, X.; Yu, X. Direct Reduction of Iron to Facilitate Net Zero Emissions in the Steel Industry: A Review of Research Progress at Different Scales. *J. Clean. Prod.* **2024**, *441*, 140933. [CrossRef]
10. Rechberger, K.; Spanlang, A.; Sasiain Conde, A.; Wolfmeir, H.; Harris, C. Green Hydrogen-Based Direct Reduction for Low-Carbon Steelmaking. *Steel Res. Int.* **2020**, *91*, 2000110. [CrossRef]
11. DRI Production. Available online: https://www.metallics.org/dri-production.html (accessed on 27 July 2024).

12. 2022 World Direct Reduction Statistics. Available online: https://www.midrex.com/wp-content/uploads/MidrexSTATSBook2022.pdf (accessed on 7 March 2024).
13. Guo, D.; Li, Y.; Cui, B.; Chen, Z.; Luo, S.; Xiao, B.; Zhu, H.; Hu, M. Direct Reduction of Iron Ore/Biomass Composite Pellets Using Simulated Biomass-Derived Syngas: Experimental Analysis and Kinetic Modelling. *Chem. Eng. J.* **2017**, *327*, 822–830. [CrossRef]
14. Xu, C.C.; Cang, D. A Brief Overview of Low CO_2 Emission Technologies for Iron and Steel Making. *J. Iron Steel Res. Int.* **2010**, *17*, 1–7. [CrossRef]
15. Ramakgala, C.; Danha, G. A Review of Ironmaking by Direct Reduction Processes: Quality Requirements and Sustainability. *Procedia Manuf.* **2019**, *35*, 242–245. [CrossRef]
16. Kirschen, M.; Badr, K.; Pfeifer, H. Influence of Direct Reduced Iron on the Energy Balance of the Electric Arc Furnace in Steel Industry. *Energy* **2011**, *36*, 6146–6155. [CrossRef]
17. Morales, R.D.; Conejo, A.N.; Rodriguez, H.H. Process Dynamics of Electric Arc Furnace during Direct Reduced Iron Melting. *Met. Mater. Trans. B* **2002**, *33*, 187–199. [CrossRef]
18. World Steel Association, Sustainability Indicators. Available online: https://worldsteel.org/steeltopics/sustainability/sustainability-indicators/ (accessed on 7 March 2024).
19. Kirschen, M.; Hay, T.; Echterhof, T. Process Improvements for Direct Reduced Iron Melting in the Electric Arc Furnace with Emphasis on Slag Operation. *Processes* **2021**, *9*, 402. [CrossRef]
20. Abolpour, B.; Afsahi, M.M.; Azizkarimi, M. Hydrogen Reduction of Magnetite Concentrate Particles. *Miner. Process. Extr. Metall.* **2021**, *130*, 59–72. [CrossRef]
21. Sanchez, J.L.G. Power Delivery from the Arc in AC Electric Arc Furnaces with Different Gas Atmospheres. *Steel Res. Int.* **2009**, *80*, 113–120. [CrossRef]
22. Ali, M.L.; Fradet, Q.; Riedel, U. Kinetic Mechanism Development for the Direct Reduction of Single Hematite Pellets in H_2/CO Atmospheres. *Steel Res. Int.* **2022**, *93*, 2200043. [CrossRef]
23. Ei-Geassy, A.A.; Shehata, K.A.; Ezz, S.Y. Mechanism of Iron Oxide Reduction with Hydrogen/Carbon Monoxide Mixtures. *ISIJ Int.* **1977**, *17*, 629–635. [CrossRef]
24. Scharm, C.; Küster, F.; Laabs, M.; Huang, Q.; Volkova, O.; Reinmöller, M.; Guhl, S.; Meyer, B. Direct Reduction of Iron Ore Pellets by H_2 and CO: In-Situ Investigation of the Structural Transformation and Reduction Progression Caused by Atmosphere and Temperature. *Miner. Eng.* **2022**, *180*, 107459. [CrossRef]
25. Sun, M.; Pang, K.; Barati, M.; Meng, X. Hydrogen-Based Reduction Technologies in Low-Carbon Sustainable Ironmaking and Steelmaking: A Review. *J. Sustain. Metall.* **2023**, *10*, 10–25. [CrossRef]
26. Liu, W.; Zuo, H.; Wang, J.; Xue, Q.; Ren, B.; Yang, F. The Production and Application of Hydrogen in Steel Industry. *Int. J. Hydrog. Energy* **2021**, *46*, 10548–10569. [CrossRef]
27. Abu Tahari, M.N.; Salleh, F.; Tengku Saharuddin, T.S.; Samsuri, A.; Samidin, S.; Yarmo, M.A. Influence of Hydrogen and Carbon Monoxide on Reduction Behavior of Iron Oxide at High Temperature: Effect on Reduction Gas Concentrations. *Int. J. Hydrog. Energy* **2021**, *46*, 24791–24805. [CrossRef]
28. Takenaka, Y.; Kimura, Y.; Narita, K.; Kaneko, D. Mathematical Model of Direct Reduction Shaft Furnace and Its Application to Actual Operations of a Model Plant. *Comput. Chem. Eng.* **1986**, *10*, 67–75. [CrossRef]
29. Hara, Y.; Sakawa, M.; Kondo, S. Mathematical Model of the Shaft Furnace for Reduction of Iron-Ore Pellet. *Tetsu-to-Hagane* **1976**, *62*, 315–323. [CrossRef] [PubMed]
30. Di, Z.; Li, Z.; Wei, R.; Liu, Y.; Meng, Q.; Chun, T.; Long, H.; Li, J.; Wang, P. Sticking Behaviour and Mechanism of Iron Ore Pellets in COREX Pre-Reduction Shaft Furnace. *Ironmak. Steelmak.* **2019**, *46*, 159–164. [CrossRef]
31. Heidari, A.; Niknahad, N.; Iljana, M.; Fabritius, T. A Review on the Kinetics of Iron Ore Reduction by Hydrogen. *Materials* **2021**, *14*, 7540. [CrossRef] [PubMed]
32. Souza Filho, I.R.; Springer, H.; Ma, Y.; Mahajan, A.; Da Silva, C.C.; Kulse, M.; Raabe, D. Green Steel at Its Crossroads: Hybrid Hydrogen-Based Reduction of Iron Ores. *J. Clean. Prod.* **2022**, *340*, 130805. [CrossRef]
33. Patisson, F.; Mirgaux, O. Hydrogen Ironmaking: How It Works. *Metals* **2020**, *10*, 922. [CrossRef]
34. Cavaliere, P.; Perrone, A.; Marsano, D. Effect of Reducing Atmosphere on the Direct Reduction of Iron Oxides Pellets. *Powder Technol.* **2023**, *426*, 118650. [CrossRef]
35. Anameric, B.; Kawatra, S.K. Properties and features of direct reduced iron. *Miner. Process. Extr. Metall. Rev.* **2007**, *28*, 59–116. [CrossRef]
36. Zhang, T.; Lei, C.; Zhu, Q. Reduction of Fine Iron Ore via a Two-Step Fluidized Bed Direct Reduction Process. *Powder Technol.* **2014**, *254*, 1–11. [CrossRef]
37. Wan, Z.; Huang, J.; Zhu, G.; Xu, Q. Numerical Simulation of the Operating Conditions for the Reduction of Iron Ore Powder in a Fluidized Bed Based on the CPFD Method. *Processes* **2022**, *10*, 1870. [CrossRef]
38. Mishra, S.; Roy, G.G. Effect of Amount of Carbon on the Reduction Efficiency of Iron Ore-Coal Composite Pellets in Multi-Layer Bed Rotary Hearth Furnace (RHF). *Met. Mater. Trans. B* **2016**, *47*, 2347–2356. [CrossRef]
39. Liang, Z.; Yi, L.; Huang, Z.; Lu, B.; Jiang, X.; Cai, W.; Tian, B.; Jin, Y. Insight of Iron Ore-Coal Composite Reduction in a Pilot Scale Rotary Kiln: A Post-Mortem Study. *Powder Technol.* **2019**, *356*, 691–701. [CrossRef]

40. Morales, R.G. Flexibility in Using Iron Ores for Direct Reduction. In Proceedings of the Metal Bulletin-2nd Latin American Steel & Iron Ore Conference, Rio de Janeiro, Brazil, April 2000; Available online: https://www.market-ing.com.mx/images/descargas/esp/MB_Paper.pdf (accessed on 27 July 2024).
41. Lu, Q.; Jiang, W.F.; Lu, C.X.; Zhao, L.G.; Yin, H.S.; Lang, J.F. Carbonising Mechanism and Carbon Distribution Behaviour during Direct Reduction in Shaft Furnace. *Ironmak. Steelmak.* **1999**, *26*, 122–126. [CrossRef]
42. Van den Berg, J.C.; Dippenaar, R.J. Fluidized-Bed Reduction of Fine Iron Ore by the in Situ Combustion of Coal. *J. S. Afr. Inst. Min. Metall.* **1989**, *89*, 89–98.
43. Komatina, M.; Gudenau, H.W. The Sticking Problem during Direct Reduction of Fine Iron Ore in the Fluidized Bed. *Metall. Mater. Eng.* **2004**, *10*, 309–328. [CrossRef]
44. Sohn, I.; Fruehan, R.J. The Reduction of Iron Oxides by Volatiles in a Rotary Hearth Furnace Process: Part I. The Role and Kinetics of Volatile Reduction. *Met. Mater. Trans. B* **2005**, *36*, 605–612. [CrossRef]
45. Nyakudya, R.Y.; Ayomoh, M. Sustainability Enhancement of the Coal Based Direct Reduction of Iron Premised on a Rotary Kiln. In *Manufacturing Driving Circular Economy*; Kohl, H., Seliger, G., Dietrich, F., Eds.; Lecture Notes in Mechanical Engineering; Springer International Publishing: Cham, Switzerland, 2023; pp. 211–218, ISBN 978-3-031-28838-8.
46. Zhu, D.; Mendes, V.; Chun, T.; Pan, J.; Li, Q.; Li, J.; Qiu, G. Direct Reduction Behaviors of Composite Binder Magnetite Pellets in Coal-Based Grate-Rotary Kiln Process. *ISIJ Int.* **2011**, *51*, 214–219. [CrossRef]
47. Wolfinger, T.; Spreitzer, D.; Schenk, J. Analysis of the Usability of Iron Ore Ultra-Fines for Hydrogen-Based Fluidized Bed Direct Reduction—A Review. *Materials* **2022**, *15*, 2687. [CrossRef]
48. Narita, K.; Kaneko, D.; Kimura, Y.; Takenaka, Y.; Tanaka, H.; Inada, Y. Production of Reduced Iron by Model Plant of Shaft Furnace. *Tetsu-to-Hagane* **1981**, *67*, 508–517. [CrossRef] [PubMed]
49. Lee, G.-Y.; Song, J.; Lee, J.-S. Reaction Kinetics and Phase Transformation during Hydrogen Reduction of Spherical Fe_2O_3 Nanopowder Agglomerates. *Powder Technol.* **2016**, *302*, 215–221. [CrossRef]
50. Efe Kinaci, M.; Lichtenegger, T.; Schneiderbauer, S. Direct Reduction of Iron-Ore in Fluidized Beds. In *Computer Aided Chemical Engineering*; Elsevier: Amsterdam, The Netherlands, 2018; Volume 43, pp. 217–222, ISBN 978-0-444-64235-6.
51. Battle, T.; Srivastava, U.; Kopfle, J.; Hunter, R.; McClelland, J. The Direct Reduction of Iron. In *Treatise on Process Metallurgy*; Elsevier: Amsterdam, The Netherlands, 2014; pp. 89–176, ISBN 978-0-08-096988-6.
52. Yang, Y.; Raipala, K.; Holappa, L. Ironmaking. In *Treatise on Process Metallurgy*; Elsevier: Amsterdam, The Netherlands, 2014; pp. 2–88, ISBN 978-0-08-096988-6.
53. Baig, S. Cost Effectiveness Analysis of HYL and Midrex DRI Technologies for the Iron and Steel-Making Industry. Master's Thesis, Duke University, Durham, NC, USA, 2016.
54. Nduagu, E.I.; Yadav, D.; Bhardwaj, N.; Elango, S.; Biswas, T.; Banerjee, R.; Rajagopalan, S. Comparative Life Cycle Assessment of Natural Gas and Coal-Based Directly Reduced Iron (DRI) Production: A Case Study for India. *J. Clean. Prod.* **2022**, *347*, 131196. [CrossRef]
55. Kumar, B.; Mishra, S.; Roy, G.G.; Sen, P.K. Estimation of Carbon Dioxide Emissions in Rotary Hearth Furnace Using a Thermodynamic Model. *Steel Res. Int.* **2017**, *88*, 1600265. [CrossRef]
56. Yang, Y.; Raipala, K.; Holappa, L. Future of Process Metallurgy. In *Treatise on Process Metallurgy*; Elsevier: Amsterdam, The Netherlands, 2014; pp. 1563–1726, ISBN 978-0-08-096988-6.
57. Ishikawa, H.; Kopfle, J.; McClelland, J.; Ripke, J. Rotary Hearth Furnace Technologies for Iron Ore and Recycling Applications. *Arch. Metall. Mater.* **2008**, *53*, 541–545.
58. Morris, A.E. Iron Resources and Direct Iron Production. In *Encyclopedia of Materials: Science and Technology*; Elsevier: Amsterdam, The Netherlands, 2001; pp. 4302–4310, ISBN 978-0-08-043152-9.
59. Soeparto, A.B. The Effect of Oxy-Carbon Injection on EAF Efficiency. Master's Thesis, University of Wollongong, Wollongong, Australia, 1996.
60. Kim, W.; Sohn, I. Critical Challenges Facing Low Carbon Steelmaking Technology Using Hydrogen Direct Reduced Iron. *Joule* **2022**, *6*, 2228–2232. [CrossRef]
61. Monsen, B.; Thomassen, E.; Bragstad, I.; Ringdalen, E.; Hoegaas, P. Characterization of DR Pellets for DRI Applications. In Proceedings of the AISTech 2015 Proceedings; Association for Iron and Steel Technology: Cleveland, OH, USA, 2015.
62. International Iron Metallics Association. Available online: https://www.metallics.org/ (accessed on 14 April 2024).
63. Small, M. Direct Reduction of Iron Ore. *JOM* **1981**, *33*, 67–75. [CrossRef]
64. Paknahad, P.; Askari, M.; Shahahmadi, S.A. Cold-Briquetted Iron and Carbon (CBIC), Investigation of Steelmaking Behavior. *J. Mater. Res. Technol.* **2020**, *9*, 6655–6664. [CrossRef]
65. Direct Reduced Iron (DRI). Available online: https://www.metallics.org/dri.html (accessed on 11 March 2024).
66. Abd Elkader, M.; Fathy, A.; Eissa, M.; Shama, S. Effect of Direct Reduced Iron Proportion in Metallic Charge on Technological Parameters of EAF Steelmaking Process. *Int. J. Sci. Res.* **2016**, *5*, 2016–2024.
67. Tappeiner, T. Ganzheitliche Betrachtung Des Einsatzes von LRI (Low Reduced Iron) Im Hochofen Zur CO_2-Minimierung. Ph.D. Thesis, Montanuniversität Leoben, Leoben, Austria, 2011.
68. Ahmed, H.; Sandeep Kumar, T.K.; Alatalo, J.; Björkman, B. Effect of Carbon Concentration and Carbon Bonding Type on the Melting Characteristics of Hydrogen-Reduced Iron Ore Pellets. *J. Mater. Res. Technol.* **2022**, *21*, 1760–1769. [CrossRef]

69. Calderon Hurtado, F.A.; Govro, J.; Emdadi, A.; O'Malley, R.J. The Melting Behavior of Hydrogen Direct Reduced Iron in Molten Steel and Slag: An Integrated Computational and Experimental Study. *Metals* **2024**, *14*, 821. [CrossRef]
70. Linklater, J. Adapting to Raw Materials Challenges: Part 1—Operating MIDREX Plants with Lower Grade Pellets & Lump Ores. Available online: https://www.midrex.com/tech-article/adapting-to-raw-materials-challenges-part-1-operating-midrex-plants-with-lower-grade-pellets-lump-ores/ (accessed on 7 March 2024).
71. Barati, M. Application of Slag Engineering Fundamentals to Continuous Steelmaking. In *Treatise on Process Metallurgy*; Elsevier: Amsterdam, The Netherlands, 2014; pp. 305–357, ISBN 978-0-08-096984-8.
72. Ma, Y.; Souza Filho, I.R.; Bai, Y.; Schenk, J.; Patisson, F.; Beck, A.; Van Bokhoven, J.A.; Willinger, M.G.; Li, K.; Xie, D.; et al. Hierarchical Nature of Hydrogen-Based Direct Reduction of Iron Oxides. *Scr. Mater.* **2022**, *213*, 114571. [CrossRef]
73. Gyllenram, R.; Sikstrom, P.; Hahne, R.; Tottie, M. *Classification of DRI/HBI Based on the Performance in the EAF A Help for Steelmaker's Procurement of Metallics*, METEC ESTAD: Düsseldorf, Germany,, 2015.
74. Tokuda, M.; Yoshikoshi, H.; Ohtani, M. Kinetics of the Reduction of Iron Ore. *ISIJ Int.* **1973**, *13*, 350–363. [CrossRef]
75. El-Geassy, A.A. Influence of Doping with CaO and/or MgO on Stepwise Reduction of Pure Hematite Compacts. *Ironmak. Steelmak.* **1999**, *26*, 41–52. [CrossRef]
76. Gonzalez, R.L.; Acosta, F.L.; Lowry, M.; Kundrat, D.; Wyatt, A.; Kuntze, J.; Fuchs, H. *Improvements in Yield in an All-DRI-Fed EAF from Minimization of FeO Generation during Melting as Well as Post-Reduction of FeO from Residual Slag*; Iron and Steel Technology: Nashville, TN, USA, 2018; pp. 36–41.
77. Manning, C.P.; Chevrier, V.F. Maximizing Iron Unit Yield from Ore to Liquid Steel (Part 2—DRI Physical Properties and DRI Handling and Storage). Available online: https://www.midrex.com/tech-article/maximizing-iron-unit-yield-from-ore-to-liquid-steel-part-2-dri-physical-properties-and-dri-handling-and-storage/ (accessed on 7 March 2024).
78. Sane, A.; Buragino, G.; Makwana, A.; He, X. Enhancing Direct Reduced Iron (DRI) for Use in Electric Steelmaking. Available online: https://www.airproducts.com/-/media/files/en/335/335-20-002-us-enhancing-direct-reduced-iron-43251.pdf (accessed on 7 March 2024).
79. Heo, J.H.; Park, J.H. Effect of Direct Reduced Iron (DRI) on Dephosphorization of Molten Steel by Electric Arc Furnace Slag. *Met. Mater. Trans. B* **2018**, *49*, 3381–3389. [CrossRef]
80. Hwang, H.-S.; Chung, U.-C.; Chung, W.-S.; Cho, Y.-R.; Jung, B.-H.; Martin, G.P. Carburization of Iron Using CO−H_2 Gas Mixture. *Met. Mater. Int.* **2004**, *10*, 77–82. [CrossRef]
81. He, Y.; Pistorius, P.C. Laboratory Carburization of Direct-Reduced Iron in CH_4-H_2-N_2 Gas Mixtures, and Comparison with Industrial Samples. *Met. Mater. Trans. B* **2016**, *47*, 1538–1541. [CrossRef]
82. Longbottom, R.J.; Ostrovski, O.; Zhang, J.; Young, D. Stability of Cementite Formed from Hematite and Titanomagnetite Ore. *Met. Mater. Trans. B* **2007**, *38*, 175–184. [CrossRef]
83. Kumar, T.K.S.; Alatalo, J.; Ahmed, H.; Björkman, B. Effect of Temperature and Gas Mixtures on Cementite Formation During the Carburization of Hydrogen-Reduced DRI. *J. Sustain. Metall.* **2022**, *8*, 1450–1464. [CrossRef]
84. Olsson, R.G.; Turkdogan, E.T. Catalitic Effect of Iron on Decomposition of Carbon Monoxide: II. Effect of Additions of H_2, H_2O, CO_2, SO_2 and H_2S. *Metall. Trans.* **1974**, *5*, 21–26. [CrossRef]
85. Fruehan, R.J. The Rate of Carburization of Iron in CO-H_2 Atmospheres: Part I. Effect of Temperature and CO and H_2-Pressures. *Met. Trans.* **1973**, *4*, 2123–2127. [CrossRef]
86. Iguchi, Y.; Endo, S. Carburized Carbon Content of Reduced Iron and Direct Carburization in Carbon Composite Iron Ore Pellets Heated at Elevated Temperature. *ISIJ Int.* **2004**, *44*, 1991–1998. [CrossRef]
87. Grabke, H.J.; Müller-Lorenz, E.M.; Schneider, A. Carburization and Metal Dusting on Iron. *ISIJ Int.* **2001**, *41*, S1–S8. [CrossRef] [PubMed]
88. Hayashi, S.; Iguchi, Y. Production of Iron Carbide from Iron Ores in a Fluidized Bed. *ISIJ Int.* **1998**, *38*, 1053–1061. [CrossRef]
89. Kim, G. Carbon Concentration and the Use of Direct-Reduced Iron in Ironmaking and Steelmaking. Ph.D. Thesis, Carnegie Mellon University, Pittsburgh, PA, USA, 2020.
90. Kim, G.; Kacar, Y.; Pistorius, P.C. Carbon Bonding State Has a Small Effect on Melting of Direct-Reduced Iron. *Met. Mater. Trans. B* **2019**, *50*, 2508–2516. [CrossRef]
91. Jess, A.; Grabke, H.; Steffen, R. *Reoxidation and Ignition Behaviour of DRI to Improve Safety*; European Commission, Directorate-General for Research and Innovation: Luxemburg, 2003.
92. Majhi, T.R. Modeling of Rotary Kiln for Sponge Iron Processing. Master's Thesis, National Institute of Technology, Rourkela, India, 2012.
93. Pietsch, N. The Influence of Raw Material and Reduction Temperature on the Structure and Characteristics of DRI. *SME-AIME* **1978**, *264*, 1784.
94. AbdElmomen, S.S. Reoxidation of Direct Reduced Iron in Ambient Air. *Ironmak. Steelmak.* **2014**, *41*, 107–111. [CrossRef]
95. Cavaliere, P.; Dijon, L.; Laska, A.; Koszelow, D. Hydrogen Direct Reduction and Reoxidation Behaviour of High-Grade Pellets. *Int. J. Hydrog. Energy* **2024**, *49*, 1235–1254. [CrossRef]
96. Paknahad, P.; Askari, M. Modeling, kinetics investigation and determining the controlling mechanisms of atmospheric oxidation of "cold" briquetted iron and carbon (CBIC). *Met. Eng.* **2021**, *23*, 206–219. [CrossRef]
97. Yazir, D.; Sahin, B.; Alkac, M. Selection of an Inert Gas System for the Transportation of Direct Reduced Iron. *Math. Probl. Eng.* **2021**, *2021*, 8529724. [CrossRef]

98. Towhidi, N. Influence of Direct Reduction Condition of Hematite Pellets with H_2/CO on the Oxidation Behaviour of DRI in Air. *Steel Res. Int.* **2003**, *74*, 595–600. [CrossRef]
99. El-Geassy, A.A.; El-Kashif, F.O.; Nasr, M.I.; Omar, A.A. Kinetics and Mechanisms of Re-Oxiation of Freshly Reduced Iron Compacts. *ISIJ Int.* **1994**, *34*, 541–547. [CrossRef]
100. Abd Elmomen, S.S. Reoxidation of Direct Reduced Iron in Stagnant Air in The Temperature Range between 150 and 450°C. *Bull. Tabbin Inst. Metall. Stud. (TIMS)* **2021**, *109*, 72–86. [CrossRef]
101. Upadhya, K. The Kinetics and Mechanism(s) of Oxidation of Direct Reduced Iron. *JOM* **1984**, *36*, 39–43. [CrossRef]
102. Medina, J.O. Studies of the Re-Oxidation Behavior of DRI in Air at Moderate Temperatures. Master's Thesis, Michigan Tech. University, Houghton, MI, USA, 1981.
103. Bandopadhyay, A.; Ganguly, A.; Gupta, K.N.; Ray, H.S. Investigations on the Anomalous Oxidation Behaviour of High-Carbon Gas-Based Direct Reduced Iron (DRI). *Thermochim. Acta* **1996**, *276*, 199–207. [CrossRef]
104. Bandopadhyay, A.; Ganguly, A.; Prasad, K.K.; Sarkar, S.B.; Ray, H.S. Determination of Kinetic Parameters for the Reoxidation of Direct Reduced Iron under Rising Temperature Conditions. *Thermochim. Acta* **1993**, *228*, 271–281. [CrossRef]
105. Hunter, R.L. *Direct Reduced Iron: Technology and Economics of Production and Use*; ISS-AIME: Warrendale, PA, USA, 1999.
106. Merki, A.; Rothberger, J.; Millner, R.; Sterrer, W. The New Age of HBI. Available online: https://magazine.primetals.com/2023/02/28/the-new-age-of-hbi/ (accessed on 11 March 2024).
107. Understanding the Different Direct Reduced Iron Products. Available online: https://gard.no/articles/understanding-the-different-direct-reduced-iron-products/ (accessed on 27 July 2024).
108. Hot Briquetted Iron (HBI). Available online: https://www.metallics.org/hbi.html (accessed on 15 April 2024).
109. Daghagheleh, O.; Schenk, J.; Zheng, H.; Taferner, B.; Forstner, A.; Rosenfellner, G. Long-Term Reoxidation of Hot Briquetted Iron in Various Prepared Climatic Conditions. *Steel Res. Int.* **2023**, *94*, 2200535. [CrossRef]
110. Nagel, H. Die Oxydation Des Eisenschwamms, Die Fakultät Für Bergbau Und Hüttenwesen Der Rheinisch. Ph.D. Thesis, Technical University of Aachen, Aachen, Germany, 1973.
111. Das, S.; Hendry, M.J. Application of Raman Spectroscopy to Identify Iron Minerals Commonly Found in Mine Wastes. *Chem. Geol.* **2011**, *290*, 101–108. [CrossRef]
112. Barrington, C. Safe Shipment of HBI—HBI C-FLEX Project & IMO Regulatory Update. Available online: https://www.midrex.com/tech-article/safe-shipment-of-hbi-hbi-c-flex-project-imo-regulatory-update/ (accessed on 2 April 2024).
113. Barrington, C. Hot Briquetted Iron-c-Flex Project: Addressing a Challenge to the HBI Value Chain. Available online: https://www.midrex.com/tech-article/hot-briquetted-iron-c-flex-project-addressing-a-challenge-to-the-hbi-value-chain/ (accessed on 3 April 2024).
114. Gray, J.; Saha-Chaudhury, N.; Sahajwalla, V. Characterisation and Corrosion of Laboratory Scale Briquettes of Reduced Iron. *ISIJ Int.* **2002**, *42*, 826–833. [CrossRef]
115. HBI C-Flex. Available online: https://hbi-c-flex.eu/ (accessed on 4 April 2024).
116. DRI Products and Applications. Providing Flexibility for Steelmaking. Available online: https://www.midrex.com/wp-content/uploads/MIdrexDRI_ProductsBrochure_4-12-18-1.pdf (accessed on 23 April 2024).
117. Ravenscroft, C.; Hunter, R.; Griscom, F. The Versatile OBM (Ore-Based Metallic): Part 2—How to Get What You Paid for: A Guide to Maintaining the Value of DRI. Available online: https://www.midrex.com/tech-article/the-versatile-obm-ore-based-metallic-part-2-how-to-get-what-you-paid-for-a-guide-to-maintaining-the-value-of-dri/ (accessed on 12 March 2024).
118. Ahmad, J.K. Inhibition of Reoxidation of Direct Reduced Iron (DRI) or sponge iron. *Int. J. Mater. Sci. Appl.* **2015**, *4*, 7–10. [CrossRef]
119. Ahmed, K.A. Inhibition of Reoxidation of Direct Reduced Iron. *ISIJ Int.* **1984**, *24*, 163–164. [CrossRef]
120. Iwamoto, I.; Kurniawan, A.; Hasegawa, H.; Kashiwaya, Y.; Nomura, T.; Akiyama, T. Reduction Behaviors and Generated Phases of Iron Ores Using Ammonia as Reducing Agent. *ISIJ Int.* **2022**, *62*, 2483–2490. [CrossRef]
121. Ma, Y.; Bae, J.W.; Kim, S.; Jovičević-Klug, M.; Li, K.; Vogel, D.; Ponge, D.; Rohwerder, M.; Gault, B.; Raabe, D. Reducing Iron Oxide with Ammonia: A Sustainable Path to Green Steel. *Adv. Sci.* **2023**, *10*, 2300111. [CrossRef] [PubMed]
122. McCafferty, E. Effect of Ion Implantation on the Corrosion Behavior of Iron, Stainless Steels, and Aluminum—A Review. *Corrosion* **2001**, *57*, 1011–1029. [CrossRef]
123. Hosokai, S.; Kasiwaya, Y.; Matsui, K.; Okinaka, N.; Akiyama, T. Ironmaking with Ammonia at Low Temperature. *Environ. Sci. Technol.* **2011**, *45*, 821–826. [CrossRef]
124. Yasuda, N.; Mochizuki, Y.; Tsubouchi, N.; Akiyama, T. Reduction and Nitriding Behavior of Hematite with Ammonia. *ISIJ Int.* **2015**, *55*, 736–741. [CrossRef]
125. Durnovich, D.; Miller, T. The Basics of DRI Plant Safety. Available online: https://www.proquest.com/openview/69da5c8a7bbaf3345542e09e2cf683de/1.pdf?pq-origsite=gscholar&cbl=1056347#:~:text=Any%20DRI%20at%20a%20temperature,more%20than%20one%20metre%20high.&text=Bins%20and%20silos%20should%20be,inert%20gas%20from%20the%20bottom.&text=Top%20slide%20gates%20should%20be%20closed%20except%20when%20DRI%20is%20being%20delivered (accessed on 11 March 2024).
126. Djadjev, I. The Evolving Law and Regulation of the Carriage of Dangerous Goods by Sea The IMDG Code and the IMSBC Code. *SSRN J.* **2015**, 1–8. [CrossRef]

127. Dutta, S.K.; Sah, R. Worldwide Direct Reduced Iron Scenario and Hazards Associated with Their Storage and Shipments. *Iron Steel Rev.* **2014**, *58*, 148–156.
128. Direct Reduced Iron (DRI). Available online: https://www.cargohandbook.com/Direct_Reduced_Iron_(DRI) (accessed on 11 March 2024).
129. Durinck, D.; Gurlit, W.; Muller, F.; van Albada, B. Closing Europe's Green-Metallics Gap. Available online: https://www.mckinsey.com/industries/metals-and-mining/our-insights/closing-europes-green-metallics-gap (accessed on 9 March 2024).
130. Sanjal, S. The Value of DRI—Using the Product for Optimum Steelmaking. Available online: https://www.midrex.com/tech-article/the-value-of-dri-using-the-product-for-optimum-steelmaking/#:~:text=versus%20Charge%20Material-,USING%20DRI,),%20and%20less%20back%20charging (accessed on 9 March 2024).
131. Voelker, B. Getting the Most from Direct Reduced Iron—Operational Results of MIDREX® Hot Transport-Hot Charging. Available online: https://www.midrex.com/tech-article/getting-the-most-from-direct-reduced-iron-operational-results-of-midrex-hot-transport-hot-charging/ (accessed on 9 March 2024).
132. Li, J.; Barati, M. Kinetics and Mechanism of Decarburization and Melting of Direct-Reduced Iron Pellets in Slag. *Met. Mater. Trans. B* **2009**, *40*, 17–24. [CrossRef]
133. Millner, R.; Rothberger, J.; Rammer, B.; Boehm, C.; Sterrer, W.; Hanspeter, O.; Chevrier, V. MIDREX H2—The Road to CO2-Free Direct Reduction. Available online: https://www.primetals.com/fileadmin/user_upload/landing_pages/2021/Green_Steel/Publications/downloads/AISTech_2021_MIDREX_H2_Final.pdf (accessed on 9 March 2024).
134. González, O.J.P.; Ramírez-Argáez, M.A.; Conejo, A.N. Mathematical Modeling of the Melting Rate of Metallic Particles in the Electric Arc Furnace. *ISIJ Int.* **2010**, *50*, 9–16. [CrossRef]
135. Gyllenram, R.; Arzpeyma, N.; Wei, W.; Jönsson, P.G. Driving Investments in Ore Beneficiation and Scrap Upgrading to Meet an Increased Demand from the Direct Reduction-EAF Route. *Min. Econ.* **2022**, *35*, 203–220. [CrossRef]
136. Pfeiffer, A.; Ernst, D.; Zheng, H.; Wimmer, G.; Schenk, J. The Behavior of Direct Reduced Iron in the Electric Arc Furnace Hotspot. *Metals* **2023**, *13*, 978. [CrossRef]
137. Morales, R.D.; Rubén, L.G.; López, F.; Camacho, J.; Romero, J.A. The Slag Foaming Practice in EAF and Its Influence on the Steelmaking Shop Productivity. *ISIJ Int.* **1995**, *35*, 1054–1062. [CrossRef]
138. Birley, R.I. *Decarbonising the DRI Feed for EAF Using H_2*; Materials Processing Institute: Sheffield, UK, 2021.
139. Turcotte, S.; Marquis, H.; Dancy, T. The Use of Direct Reduced Iron in the Electric Arc Furnace. In *Electric Furnace Steelmaking*; AIME, Iron Steel Society: Warrendale, PA, USA, 1985; pp. 115–126.
140. Kieush, L.; Schenk, J.; Koveria, A.; Hrubiak, A.; Hopfinger, H.; Zheng, H. Evaluation of Slag Foaming Behavior Using Renewable Carbon Sources in Electric Arc Furnace-Based Steel Production. *Energies* **2023**, *16*, 4673. [CrossRef]
141. Kieush, L.; Schenk, J. Influence of Carbon Material Properties on Slag-Foaming Dynamics in Electric Arc Furnaces: A Review. *Steel Res. Int.* **2024**, 2400235. [CrossRef]
142. Kieush, L. Coal Pyrolysis Products Utilisation for Synthesis of Carbon Nanotubes. *Pet. Coal* **2019**, *61*, 461–463.
143. Kurecki, M.; Meena, N.; Shyrokykh, T.; Korobeinikov, Y.; Jarnerud Örell, T.; Voss, Z.; Pretorius, E.; Jones, J.; Sridhar, S. Recycling Perspectives of Electric Arc Furnace Slag in the United States: A Review. *Steel Res. Int.* **2024**, 2300854. [CrossRef]
144. Memoli, F. Behavior and Benefits of High Fe_3C-DRI in the EAF. *Iron Steel Technol.* **2019**, *2*, 1928–1945.
145. Lule, R.; Lopez, F.; Espinoza, J.; Torres, R.; Molares, R.D. The Production of Steels Applying 100% DRI for Nitrogen Removal, the Experience of ArcelorMittal Lazaro Cardenas Flat Carbon. In Proceedings of the AISTech 2009—Iron and Steel Technology Conference, St. Louis, MO, USA, 4 May 2009; Volume 1, pp. 489–498.
146. Dutta, S.K.; Lele, A.B.; Pancholi, N.K. Studies on Direct Reduced Iron Melting in Induction Furnace. *Trans. Indian Inst. Met.* **2004**, *57*, 467–473.
147. Hassan, A.; Kotelnikov, G.; Abdelwahed, H. Melting Characteristics of Alternative Charging Materials in an Electric Arc Furnace Steelmaking. *Ironmak. Steelmak.* **2021**, *48*, 1136–1141. [CrossRef]
148. Song, S.; Zhao, J.; Pistorius, P.C. MgO Refractory Attack by Transient Non-Saturated EAF Slag. *Met. Mater. Trans. B* **2020**, *51*, 891–897. [CrossRef]
149. Heo, J.; Park, J.H. Interfacial Reactions between Magnesia Refractory and Electric Arc Furnace (EAF) Slag with Use of Direct Reduced Iron (DRI) as Raw Material. *Ceram. Int.* **2022**, *48*, 4526–4538. [CrossRef]
150. Heo, J.; Park, J.H. Effect of Temperature on the Slag/Refractory Interfacial Reaction with Directed Reduced Iron (DRI) Addition in an Electric Arc Furnace (EAF) Process: Diffusional Growth of Magnesiowüstite Layer by Boltzmann-Matano Analysis. *Ceram. Int.* **2022**, *48*, 17217–17224. [CrossRef]
151. Mulholland, E.W.; Hazeldean, G.S.F.; Davies, M.W. Visualization of Slag-Metal Reactions by X-RAY Fluoroscopy: Decarburization in Basic Oxygen Steelmaking. *J. Iron Steel Inst.* **1973**, *211*, 632–639.
152. Min, D.-J.; Fruehan, R.J. Rate of Reduction of FeO in Slag by Fe-C Drops. *Met. Trans. B* **1992**, *23*, 29–37. [CrossRef]
153. Goldstein, D.A.; Fruehan, R.J.; Oztruk, B. The Behaviour of DRI in Slag-Metal Systems and Its Effect on the Nitrogen Content of Steel. *Iron Steelmak.* **1999**, *26*, 49–61.
154. Sharifi, E.; Barati, M. The Reaction Behavior of Direct Reduced Iron (DRI) in Steelmaking Slags: Effect of DRI Carbon and Preheating Temperature. *Met. Mater. Trans. B* **2010**, *41*, 1018–1024. [CrossRef]
155. Kiasaraei, E.S. Decarburization and Melting Behavior of Direct-Reduced Iron Pellets in Steelmaking Slag. Master's Thesis, University of Toronto, Toronto, ON, Canada, 2010.

156. Murthy, G.G.K.; Sawada, Y.; Elliott, J.F. Reduction of FeO Dissolved in CaO-SiO_2-Al_2O_3 Slags by Fe—C Droplets. *Ironmak. Steelmak.* **1993**, *20*, 179–190.
157. Sadrnezhaad, K. Direct Reduced Iron: An Advantageous Charge Material for Induction Furnaces. *J. Eng.* **1990**, *3*, 37–47.